MICROFLUIDIC RESEARCH TOOLS FOR NEUROSCIENCE

by

Raheel Samuel

A dissertation submitted to the faculty of
The University of Utah
in partial fulfillment of the requirements for the degree of

Doctor of Philosophy

Department of Mechanical Engineering

The University of Utah

August 2014

The University of Utah Graduate School

STATEMENT OF DISSERTATION APPROVAL

The dissertation of **Raheel Samuel**

has been approved by the following supervisory committee members:

Bruce Gale	, Chair	**3/7/2014** Date Approved
Meredith Metzger	, Member	**3/7/2014** Date Approved
Stacy Bamberg	, Member	**3/7/2014** Date Approved
Carlos Mastrangelo	, Member	**3/7/2014** Date Approved
Michael Redd	, Member	**3/7/2014** Date Approved

and by **Tim Ameel** , Chair/Dean of

the Department/College/School of **Mechanical Engineering**

and by David B. Kieda, Dean of The Graduate School.

ABSTRACT

Microfluidics is an emerging field that deals with the technology and science of manipulation of fluid in microchannels. Since its birth in the 1990s, it has now gradually matured into an enabling technology, like microelectronics and software engineering. A majority of current applications of microfluidics are in life sciences.

Polydimethylsiloxane (PDMS) is a soft elastomer and a popular material for fabricating microfluidic devices. This is due to PDMS's unique set of material properties and low cost. Furthermore, the unique mechanical properties of thin PDMS layers/membranes (< 200 μm) can be used to increase the functionality of PDMS-based microfluidic systems. In this presentation, three unique neuroscience applications of PDMS-based microfluidic devices are presented. The working principle behind each of these devices depends on the unique properties of thin PDMS layers.

In the first project a fabrication protocol was developed to stack 30 patterned 10-μm thick PDMS layers on top of each other without any trapped air bubbles or wrinkles. Each PDMS layer was patterned by spin-coating uncured PDMS on a photolithographic micromold at very high spin speeds and thermally curing the layer later. The layer stacking procedure was done manually using no specialized tools and did not cause any layer deformation to inhibit functionality. This fabrication protocol was used to develop the first ever microfluidic Magnetic Resonance Imaging Phantom to stimulate brain white matter.

In the second project, laser ablation was used to rapidly prototype micromolds and by using these micromolds a unique cation protocol was developed and characterized to build microvalve arrays (consisting of 100s of microvalves) without access to any cleanroom facility. This was achieved by manipulating the stiffness of thin PDMS layers that are inherent part of pneumatic microvalves. These microvalve arrays were used to build a microfluidic platform for manipulation of *C. elegans* (a type of a small round worm), which are used extensively for neuronal behavioral analysis.

In the last project using similar fabrication techniques (as described in the second project) microfluidic genotyping devices are developed for zebrafish embryos that are less than 2 days old. The unique advantage of the microfluidic zebrafish genotyping devices is that they enable researchers to collect genetic material (for genotyping) from a zebrafish embryo (1 to 2 days old) without causing any harm to its health. This capability is not possible with any other model multicellular organism to date. The working principle behind one of the presented genotyping devices depends on the controlled actuation of PDMS membranes.

TABLE OF CONTENTS

ACKNOWLEDGEMENTS

I would first like to thank God for his love and grace through his son Jesus Christ; the source of all truth and grace. I thank God for my wonderful family who believed in me ever since I was born. Children are born with unique skills but it is up to their parents to help them discover those skills at an early age so they can master them further. Similarly I am thankful to the love and support of my dear sisters.

I am thankful to my Advisor (Dr. Bruce Gale) for his support and care in training me for my future career. The life of a PhD student depends a lot on the quality of mentorship of the PhD advisor. I am privileged to be one of his PhD students.

I am thankful to my beautiful fiancée, the woman that I have been in love with for the last 8 years, Leena. Without her support, patience, and love I would not have been able to finish my PhD.

I would like to thank members of Gale's Lab, the Department of Mechanical Engineering, Bonkowsky's Lab, Wittwer's Lab and all other people (that are somehow associated with The University of Utah) who supported me in my PhD program. I am humbled by their unconditional service to me.

I want to thank a very dear friend of mine, Fahad Saeed, for his support and encouragement. Without his friendship, I may not have made it to the US for my graduate career.

In the end I would like to thank all the Christian community in Salt Lake City that I

have been blessed with. This especially includes friends associated with Utah Bridges International, Intervarsity Christian Fellowship, Cross Culture Club, and Missio Dei Community Church. Though the last 5 years of my life have been professionally enriching, I have grown very much in spirit and character through these loving people.

Thank you, thank you so much.

CHAPTER 1

INTRODUCTION

Microfluidics – the Enabling Technology

Microfluidics is an interdisciplinary subfield of micro-electromechanical systems (MEMS) and is described by George M. Whitesides, a microfluidics expert as follows, "Microfluidics deals with the scientific and technological manipulation of small amounts of fluids (10^{-9} and 10^{-18} liters) using channel dimensions in the scale of tens to hundreds of micrometers" [1]. Most current applications of microfluidics are in the fields of biological and chemical analysis for which the physics of microfluidics provide unique advantages [1]. Analyzing fluid samples at the microscale has a number of advantages: small amount of samples and reagents used, high-throughput and device sensitivity, extremely short time for analysis, and all of this realized in a compact, low cost device [1]. Microfluidics, like many promising technologies had its initial expectations hyped in the 1990s, which, however, died down over a couple of years [2]. Since the year 2005, though, microfluidics has been gradually maturing as an "enabling technology," much like software engineering and microelectronics that are used as tools in the growth of other technologies or disciplines [2].

Microfluidics for Neuroscience

One of the emerging fields of applied research that could greatly influence the progress of human society (from 2010–2060) is "Neurotechnology"—a combination of actuation, imaging, and other analytical tools that have the ability to influence the human central nervous system, particularly the brain [3]. Neurotechnology stems from neuroscience, which seeks to answer questions related to the structure of the nervous system, human cognition abilities, and treatment/diagnosis/prevention of neurobiological and mental diseases. Microfluidics is gradually becoming an enabling tool for the growth of neuroscience [4], [5]. According to a recent review article [4], microfluidic-based neuroscience tools can be divided into six categories: (1) neuron culture, (2) neuron manipulation, (3) neural stem cell differentiation, (4) neuropharmacology (or study of drug-induced effects and cell functionality in the nervous system), (5) neuroelectrophysiology (study of ionic currents and electrical phenomena in neurons and nerve tissue), and (6) neuron biosensors. Despite the diversity of all of the above applications, they all basically take advantage of the "controlled microenvironment" that can be generated using microfluidics. A controlled microenvironment provides three advantages: (1) it can help confine a neuron to a particular physical/biochemical space and help in neuron growth, (2) provide controlled release and controlled exposure to different physical stimulations, and (3) be able to measure the output signals from neurons or neural tissue with high sensitivity and low noise.

These advantages of a controlled microenvironment have recently caught the attention of researchers that use Caenorhabditis elegans (*C. elegans*) and Zebrafish

(*Danio rerio*) as model multicellular organisms to answer key questions in neurobiology. Biomedical research involving microsystems and Zebrafish as a model organism has been reviewed in Chapter 4 of this dissertation. In this section a brief review is provided on microsystems involving *C. elegans*.

C. elegans are a type of round worm that are about 1-mm long and 50 μm in diameter and are naturally found in temperate soils. *C. elegan* is popularly used for neuronal-behavior studies [6]. Microfluidic devices for research involving *C. elegans* are usually referred to as worm-chips [7]. These worm-chips can be broadly defined in four categories of application: worm manipulation, worm immobilization and imaging, behavioral studies, and laser microsurgery.

Because of the worm's small size, manual worm handling is tedious and slow when the numbers of worms reaches thousands. Furthermore, manual worm handling is stressful for the worms, which is not ideal for behavioral studies. In worm-chips, worms can transported in microchannels from one place to another while suspended in a buffer solution. This mode of movement is very similar to their natural locomotion and is therefore less stressful. Secondly, microfluidics can be coupled with programmed microelectronic hardware to make worm manipulation less tedious by incorporation of a certain degree of automation.

In certain studies when *C. elegans* need to be imaged, they have to be immobilized. The degree of immobilization depends on the resolution of the image or video. Before microfluidics, worms were anesthetized or glued on coverslips. These methods, however, affected the physiology of the worm and impacted the results of the studies concerned [7]. Now worm-chips have been designed to enable high-resolution imaging

of worms while immobilizing them either by cooling, CO_2 exposure, gelation of the fluid surrounding the worm, or by physical restriction/compression [7].

The combination of worm manipulation, imaging, and immobilization in microfluidics has resulted in ability to perform screens of thousands of worms in a high-throughput fashion for neurobiological research [7] and has made microfluidics an important asset for worm labs. Furthermore, aided with worm manipulation and immobilization techniques, worm-chips have been made to provide controlled chemical or physical stimuli to worms for neuronal behavior studies and laser ablation at the cellular level [7].

The functionality of any microfluidic system has to take into the consideration the fabrication material. Based on the material, microfluidic engineers can achieve the appropriate design of the device and overcome associated fabrication constraints. The next section discusses a material popularly used in the fabrication of microfluidic systems, especially for rapid prototyping.

Polydimethylsiloxane (PDMS) – the Star Material for Microfluidics Research

Polydimethylsiloxane (PDMS) is a biocompatible elastomer that is popularly used as a fabrication material for microfluidic devices including microfluidic-based tools for neuroscience [4]. PDMS is cost-effective, has good optical transparency and gas permeability, and facilitates rapid prototyping [8]. Microfluidic structures from PDMS are produced using a variety of methods that can be all classified as “soft lithography” [9]. One great benefit of soft lithography techniques is that they provide an opportunity

to bring fabrication of microfluidics outside the cleanroom. This ability to use PDMS in "normal" environments reduces costs and makes fabrication simpler while maintaining the desired functionality of the microfluidic device, which is an important attribute for creating an impact for microfluidics as an enabling technology.

A common soft lithography technique used for making PDMS devices is replica molding [9]. In replica molding a master mold is prepared using a specific set of materials and methods. Then PDMS (a mixture of base and curing agent) is poured over the master mold and cured by thermal treatment. Once PDMS is cured it can be physically separated from the master mold and contains a negative relief pattern of the master mold. A major part of this dissertation focuses on the innovative utilization of special mechanical properties of PDMS spin-cast layers (< 200 μm thickness) to make fabrication of PDMS-based microfluidics simpler and cost effective. Therefore, it is necessary to review current applications of such layers.

There are currently two methods to produce thin PDMS layers (< 200 μm): the membrane sandwich method [10]–[12] and the spin casting method [13]. In the membrane sandwich method, the uncured PDMS is placed between a master mold and a flat plate and squeezed by application of pressure through clamps. The desired thickness of PDMS layer can be achieved by regulating the pressure accordingly or using physical stops for the process. The entire assembly is placed in an oven that cures the PDMS layer to the required thickness. In the spin casting method, uncured PDMS is spun on a wafer at high speeds so that PDMS spreads as a layer on the wafer. The thickness of the layer can be controlled by varying the spin speed of the wafer; an increase in spin speed would produce a decrease in layer thickness. Recently a remarkable presentation

demonstrated a drastic increase in mechanical strength and thermal stability of spin-cast PDMS layers when layer thickness reaches a critical thickness value (200 μm) [14]. Therefore spin-cast PDMS layers with thickness less than 200 μm would inherently have a higher Young's Modulus than thicker PDMS layers. This modulus increase occurs because of the reordering of polymer chains in the radial direction of the PDMS substrate at high spin speeds [14]. The strength and flexibility of spin-cast PDMS layers has proven to be a valuable asset in the development of microfluidic devices.

These layers have been used to make 3D microfluidic systems. The basic procedure is to develop an SU-8 mold using a silicon substrate and spin coat PDMS on top. Later, the thin peeled-off PDMS layers (which are perforated) are used as interconnects between thicker PDMS slabs with molded channels for 3D channel realization. Luo et al. developed a perforated membrane using a SU-8 mold with micropillars [13]. The PDMS layer had a thickness lower than the protruding micropillars: about 40–50 μm. The pillars are removed using a scalpel and a sticky tape which leaves behind a perforated PDMS layer. However, a more efficient method for fabricating perforated PDMS layers has been developed by Kang et al. [15]. The method is very similar to Lou's; the only difference is that SU-8 micropillars are retained, and a thin uncured PDMS layer that just covers the micropillars' top is blown off by air or nitrogen through a pressurized needle. The entire PDMS layer is then cured and later peeled off to yield a perforated layer. Nonetheless, both of these fabrication processes can be laborious for fabricating highly perforated PDMS membrane.

PDMS membranes that are fabricated by spin coating techniques can reach thicknesses down to 70 nm [16]. Some spin-cast thin PDMS membranes have been used

as key functioning elements for continuous biomechanical testing of soft tissues [17]. Load-deflection studies have been carried out on spun PDMS membranes as thin as 493 nm [18]. Key observations included an increase in flexibility of the membranes with decrease in thickness and increase in base ratios (with respect to curing agent).

PDMS layers as thin as 4 μm have been used to fabricate microlens arrays [19]. The idea is to pattern the PDMS layer using a Parylene C lift-off technique. A 15-μm thick Parylene C layer is first deposited on a silicon substrate by chemical vapor deposition. The Parylene C layer is patterned using a photoresist masking layer followed by dry etching. Uncured PDMS is then spun on the Parylene C layer and partially cured. Finally, the Parylene C layer is carefully peeled off leaving behind patterned PDMS membranes on the surface of the substrate.

Microvalves and micropumps are important integral parts of microfluidic systems. There have been many designs of microvalves in the past [20], and among them are designs based on actuation of PDMS membranes for fluid flow regulation. Basically the flexible thin membrane is distended by an actuator (thermopneumatic, pneumatic, or phase change actuator) that seals off a microchannel and stops the flow.

Some of these are active mechanical microvalves that are thermopneumatically actuated by heating trapped air above or below the membrane (depending upon the position of the pressure chamber), which later expands and deflects the membrane to regulate fluid flow [21]. Similarly there are external pneumatically actuated PDMS membrane microvalves that employ the same membrane actuation principle [20]. The thicknesses of the PDMS membranes in these microvalves range between 3 μm to 200 μm. Thin membranes are preferred because they provide more deflection per unit power

consumption (for microheaters). There are nonmechanical PDMS membrane microvalves that also work on the membrane actuation principle, but use the characterized volumetric expansion of hydrogels as the actuation source [22].

Micropumps based on the function of reciprocating membranes are called reciprocating displacement pumps. The diaphragm/membrane comes into direct contact with the pumping fluid. The driver could be any type of actuator: piezoelectric, electromagnetic, thermopneumatic, pneumatic, or electrostatic. There are a few practical demonstrations of PDMS membrane micropumps with pneumatic actuation [23], [24].

PDMS tends to swell in organic solvents [25], which is one of the main factors for the limiting use of PDMS as a fabrication material for microfluidic systems for chemical analysis [1]. Researchers have been able to reduce the swelling of PDMS in organic solvents by introducing fillers in PDMS, called zeolites [26]. These fillers increase the cross-linking density of PDMS, which in turn decreases the swelling tendency of the polymer network. Such modified PDMS membranes have been used in nanofiltration in highly swelling solvents like ethlyacetate and toluene.

Remarkably, some researchers have used the swelling of PDMS to produce complex nanostructures on gold substrates [27]. Zhang et al. have used a sequence of steps that includes controlled swelling of patterned PDMS layer with a Fe_2O_3 nanoparticles dissolved in an organic solution. Furthermore, the paper reports on the characterization of swelling of PDMS, which thereby enables researchers to vary the aspects of the transferred pattern (e.g., nanofeature's size and shape).

Conductive thin PDMS layers (25-μm thick) have been made by Ion Implantation of gold, palladium, and titanium to form Dielectric Elastomer Actuators [28]. The layers

retain electrical conductivity up to strains of 175% and cyclical straining at 30% for 105 cycles. The principle working aspect of these conductive layers is the formation of nanosized ion clusters on top of the layer. These clusters touch each other for electrical conduction. Furthermore, when the layer is stretched, the clusters slide over each other while maintaining electrical contact. In contrast, polymer electrodes formed by sputter deposition of conductive metal can only withstand strains up to 1% before turning nonconductive.

Recently, the fabrication technology and the concept of membrane displacement micropumps and membrane micro-optics have been used by researchers to make adaptable microlenses and micromirrors. Schneider et al. have fabricated and characterized an adaptive PDMS-membrane lens with an integrated piezo actuator [29]. The distended thin PDMS membrane (30–1250 μm thickness) with characterized optical properties was used as a lens material. The membrane was distended by an integrated piezo actuator that pumps water/oil beneath the membrane.

In a similar setup, configurable liquid-membrane microlenses have been fabricated by distending a 50-μm thick PDMS membrane [30]. However, in this case the pumping fluid itself is a refractive liquid with known optical properties. Micropumping of the refractive liquid was done with external hydrostatic pumps.

Hongbin et al. have built solid microlenses using the same principle of distending thin PDMS membranes (30-μm thick) by external pumping (syringe pumps), but the pumping fluid itself is uncured PDMS [31]. After distending the membrane to the required level, the pressure is kept constant, and the uncured PDMS is thermally cured, forming a solid PDMS microlens. A number of microlenses with distinct focal lengths

can be formed by simply varying the applied pressure.

Tunable micromirrors have been fabricated by utilizing the deflection of thin PDMS membranes [30]. The micromirror (a silicon hinged cantilever with evaporated aluminum on top) was bonded to the membrane, which was deflected by thermopneumatic pump actuators. The gas permeability of PDMS membranes inhibited consistent applied pressure, which is important in positioning the micromirror. This permeability was controlled by depositing (Low Temperature Chemical Vapor Deposition) a 0.7μm thick layer of Parylene on top of the PDMS membrane.

The potential of thin PDMS layers and membranes has just caught the attention of the microfluidics research community, but the signs are that these thin membranes/layers will be used more in microelectromechanical systems (MEMS), especially in cheap, disposable microfluidics systems. However, since current MEMS fabrication processes rely heavily on the alignment of planar structured layers, the alignment of patterned thin PDMS layers with respect to substrates can help in realizing more applications of thin PDMS layers in MEMS. For in MEMS any thin material that is strong [14], flexible [14], conformable [1], biocompatible [8], cheap [1], thermally stable [14], and has characterized optical properties [29] can be of significant value. The next section introduces a fabrication protocol that utilizes these unique properties of thin PDMS layers to make a uniquely structured microfluidic device for magnetic resonance imaging: a popular tool used in neuroscience.

Fabrication of a Microfluidic Phantom for Diffusion Tensor Magnetic Resonance Imaging (DT-MRI) from Patterned Thin PDMS Layers

Diffusion Tensor Magnetic Resonance Imaging (DT-MRI) is used to measure the diffusivity of water and metabolites noninvasively in the microdomain [32], [33]. Hence, DT-MRI is highly applicable in neuoroscience and medicine that involves analysis in stroke, brain development, demyelinating disorders, and tumor imaging [34].

DT-MRI machines generate these detailed images by measuring the restricted Brownian motion of water molecules (also termed as anisotropic diffusion) [34]. In biomedical applications anisotropic diffusion is present in white matter, cartilage, muscle, and in the eye's lens [34]. In the quantitative validation of MRI machines, physical models (that could be scanned in MRI machines) are required with predefined microscopic architecture. The microscopic architecture of these phantoms constrains the motion of the water molecules leading to anisotropic diffusion, which is then observed using MRI. Scanning these physical phantoms using DT-MRI machines can be used in validating MRI technology by comparing the measured results with the known physical structure, allowing fine tuning of computer algorithms working behind the imaging hardware. Researchers have been able to fabricate artificial fiber diffusion phantoms using rayon, polyethylene, polyester, polyamide, linen, and hemp [35], but these phantoms are difficult to reproduce with consistency in the microscopic architecture, a highly important factor in quantitative validation of MRI machines.

However, with microfabrication techniques reproducible phantoms could be fabricated. Previously, a microfluidic MRI phantom has been developed to simulate

blood perfusion in tissues [36], but no microfabricated phantoms have been reported in the literature to simulate brain white matter, most likely because of the fabrication challenges associated with the complicated design of such phantoms.

This dissertation introduces a unique fabrication process for stacking 30 patterned 10-μm thick PDMS layers to create a Diffusion Tensor Magnetic Resonance Imaging (DT-MRI) phantom, which can be used as a physical model for calibration and standardization of DT-MRI machines. Each layer consists of thousands of microchannels with a 5 μm x 5 μm cross-section that are intended to direct or limit diffusion to directions primarily along the length of the channels (called anisotropic diffusion). Using the Einstein Diffusion equation, in a period of 100 ms (time duration of a typical Diffusion Weighted image shot), a water molecule at 25 ºC would cover a mean-squared distance of 1.32 μm^2 [37], [38]. The water molecules that are closer to the channel walls are more likely to diffuse along the channel. Hence, based on the mean-square distance of 1.32 μm^2, about 40% of the channel volume (of a 5 μm x 5 μm cross-section channel) consists of molecules that are more likely to diffuse along the channel. This provides us with a rough idea about the percentage of water molecules that are most likely to generate an appropriate MRI signal. Smaller channels (close to 1 μm^2 in cross-sectional area) would facilitate a better degree of anisotropic diffusion and consequently increase the percentage of water molecules producing a favorable MRI signal, but this would include additional fabrication complications.

This fabrication process and associated results have been published in a journal [35]. Furthermore, the ability to stack multiple layers of patterned thin PDMS layers to form PDMS laminates would help in increasing the functionality of PDMS-based

microfluidic devices.

Fabrication of all-PDMS Microvalve Arrays with Application to *Caenorhabditis Elegans (C. elegans)* Manipulation

Since PDMS is a soft elastomer, it can be used to make micropneumatic valves and pumps [39]—essential in most integrated microfluidic devices and difficult to fabricate in rigid materials like silicon and glass. At the microscale, flexible PDMS layers can act as diaphragms to pump/regulate fluid flow in micropumps and valves, based on layer displacement. In this dissertation a soft lithography method is introduced in which the mechanics of spin-cast PDMS layers are manipulated to design a simple and cost-effective protocol for fabricating pneumatic microvalve arrays. Currently, only two types of pneumatically actuated microvalves can be built in PDMS substrates: Quake valves and doormat-style valves [39]. Both valves use an actuating membrane to regulate the flow of fluid in the microchannel. Quake valves require a rounded microchannel cross-section profile and function best for shallow channels [39]. When Quake valves are produced in large numbers, because of the rounded microchannel cross-section profile, either cleanroom facilities or complicated fabrication protocols are required [39]. Doormat-style valves are easier to incorporate in PDMS-based microfluidics as they can be produced with any microchannel cross-section profile. So master molds for microfluidics requiring doormat-style valves can be made outside the cleanroom by knife cutting of adhesive vinyl films [40]. However, doormat-style valves are harder to produce in arrays because the valve-seat needs to be protected from the required oxygen/air plasma exposure during the fabrication process. However, by

utilizing the strength and manipulating the stiffness of thin PDMS layers a fabrication protocol for producing hundreds of doormat-style valves was designed and developed. This new fabrication protocol was used to develop a microfluidic high-throughput screening manifold (in PDMS) for *C. elegans* that can be coupled with standard fluorescence imaging hardware for phenotype-based screens.

The high-throughput screening manifold was built by PDMS-based replica molding. Despite the ease of producing microfluidic devices using PDMS replica molding, the fabrication of the required micromolds has always been tedious or expensive when rapid prototyping is required during design iterations. This underscores the cost-effectiveness and rapid prototyping capabilities of PDMS-based replica molding.

A common process of fabricating micromolds for replica molding is by photolithographic processes that require expensive cleanroom facilities. This process can produce molds at high resolutions with smooth surfaces. However, in some cases this may not be a requirement or even a disadvantage in terms of costs when rapid prototyping is required in design iterations. Therefore in order to circumvent this limitation of micromolds for replica molding, microfluidic engineers have developed various other techniques.

Among these techniques are the ones that have more moderate costs: solid-object printing and Computer Numerical Control (CNC) machining [41]. Making molds from CNC machining is tedious (and consequently expensive) when alterations in design are required frequently. Solid-object printing technology is not tedious, can have good resolution for micromolding, and is gradually becoming cheaper and therefore provides a good means to prototype micromolds. One limitation of solid-object printing for

making micromolds can come from the quality of surface finish. For example, after printing, parts require significant cleaning and may be relatively rough. Another limitation comes from the thermal curing process of PDMS once poured over the mold; insufficient thermal stability of the solid-object printed mold can lead to fracture under the release forces experienced by the mold during release of the cured PDMS part. However, as solid-object printing improves, these limitations may soon be overcome.

Micromolds have also been made using Printed Circuit Boards (PCBs), without the use of a cleanroom [42]. However, they still require some photolithography and associated wet etching.

There are also other simpler methods where micromolds are made by simply printing (an office printer or a photocopy machine) structures on a transparency [41]. Bartholomeusz et al. developed a similar technique of making micromolds but used patterned adhesive vinyl films as the material for microstructures on the mold [40]. The patterning of these films was done by transferring a 2D CAD drawing to a cutting plotter that then cuts the film to generate the pattern. The pattern was then transferred to a Petri dish or a flat container to fully realize the micromold. But the simplicity of these techniques comes with the cost of high surface roughness and poor resolution of printed microstructures as compared to a micromold generated by photolithography. However, all of these techniques demonstrate an application in biomedical microfluidics. Therefore, the suitability of a micromold fabrication method depends on the application and the budget involved. Having diverse options to build the same microfluidic device is always advantageous.

In this work the micromold for the high-throughput screening manifold was built by

laser ablation (patterning) of adhesive vinyl films [43]; these patterned films are then placed in Petri dishes to fully fabricate the micromolds. In laser ablation, photons are absorbed by the material (that is being processed), which increases in temperature, consequently evaporating the material. Fabrication of microfluidic devices by laser ablation of metals, glass, polymers, and ceramics is popular in the microfluidics research community [44] because there is a wide choice of fabrication materials that can be processed with lasers, the cost per unit is low, and fabrication times are short due to high laser scanning speeds and high laser intensities [44]. Laser ablation of adhesive vinyl films as compared to knife cutting used by Bartholomeusz et al. [40] and can produce microstructures at a higher resolution and more complicated microchannel geometries.

Microfluidic Zebrafish Genotyping Chips

As part of work reported in this dissertation, a pair of zebrafish genotyping chips are reported. These chips require multirelief master molds that contain multiple levels of relief. Fabrication of multirelief master micromolds by standard photolithography is tedious, difficult, and requires a cleanroom facility, but microfluidic circuits with varying microchannel heights can help build unique solutions [45]. Currently, such molds are only available by solid-object printing technology [46], expensive stereo lithography [47], tedious reaction-diffusion [47], and by use of expensive femtosecond lasers (ultra-short-pulse laser) for localized 3D ablation in glass [48] and PDMS [49]. In solid-object printing technology, these molds are thermally unstable due to a combination of PDMS curing temperatures and the forces experienced by the mold

during the separation of cured PDMS from the mold. In addition, master molds from solid-object printing do not have a smooth surface finish, which is essential for replica-molded PDMS devices that need to bond to each other or other smooth substrates for the final realization of microfluidic devices. CO_2 laser (a type of Infrared laser) systems are among the low-priced laser systems and have been popularly used in micromachining microfluidic structures in PMMA and adhesive films [43]. Luo et al. utilized the cost-effectiveness of CO_2 laser systems to fabricate microfluidic circuits from adhesive films with microchannels of varying height. This fabrication method was achieved by controlling the depth of laser ablation at different sections of a 2-dimensional CAD (computer aided design) drawing.

In this dissertation a similar fabrication method is used to build two types of microfluidic devices that aid in the collection of genetic material for genotyping of zebrafish embryos (1–2 day old) while keeping the embryos 100% viable, which is not currently possible with any model multicellular organism). In addition, the working principle behind one of these genotyping devices is the deflection of a PDMS membrane that clips a small part of the embryo's tail without harming it. The design of actuation of this PDMS membrane is based on the model developed in the work described in Chapter 3. It should be noted that zebrafish are a powerful vertebrate model widely used by neurobiologist to study genetically acquired diseases [50]. More information on microfluidics for zebrafish research will be presented in Chapter 4.

Summary

With special focus on problems related to neuroscience and application of thin PDMS layers (< 200 μm) this dissertation introduces three microfluidic devices with their unique set of technological and scientific contributions. Chapter 2 describes the development of a microfluidic MRI phantom that can be used to improve the imaging algorithms of MRI machines. The microfluidic phantom was a multilayer structure consisting of 30 patterned 10-μm thick PDMS layers. The challenge was to develop a fabrication protocol in which each of these layers could be separately made and bonded on top of each other without any wrinkles, damage, and trapped air bubbles.

Chapter 3 introduces a fabrication protocol to make an array of hundreds of doormat-style microvalves outside a cleanroom facility, which was achieved by manipulation of PDMS membranes incorporated in the design of these microvalves. Design analysis was performed using simulations and experiments so as to determine key design parameters of the microvalves to get optimum valve yield. The microvalve fabrication technology developed in this work was used to make a microfluidic high-throughput genetic screening manifold in PDMS for *C. elegans*. *C. elegans* is a model organism used by scientists for neurobiological studies.

Chapter 4 reports on the use of laser ablation of adhesive vinyl films to fabricate multirelief micromolds for PDMS-based replica molding with applications in zebrafish genotyping. The chapter presents two microfluidic devices that have the capability to collect genetic material from zebrafish embryos (1 to 2 day old) without having any effect on embryo viability. Zebrafish are a model organism used by scientists to answer key questions in neurobiology and cancer research. Using the genetic material,

zebrafish embryos can be genotyped at an early age and be available for further studies. This work also describes procedures and results for the determination of device sensitivity and embryo viability. As with the other chapters, a key element in the design of one of these genotyping devices is the controlled deflection of a PDMS membrane.

Chapter 5 provides a conclusion for the dissertation highlighting the knowledge gained from all three dissertation-projects, scientific and technological contributions, and areas where further research can be meaningfully pursued.

References

[1] Whitesides, G. M., 2006, "The Origins and the Future of Microfluidics," Nature, **442**(7101), pp. 368–373, doi: 10.1038/nature05058

[2] Becker, H., 2009, "Hype, Hope and Hubris: The Quest for the Killer Application in Microfluidics," Lab Chip, **9**(15), pp. 2119–2122, doi: 10.1039/b911553f

[3] Lynch, Z., 2004, "Neurotechnology and Society (2010 – 2060)," Ann. N. Y. Acad. Sci., **1013**, pp. 229–233, doi: 10.1196/annals.1305.016

[4] Wang, J., Ren, L., Li, L., Liu, W., Zhou, J., Yu, W., Tong, D., and Chen, S., 2009, "Microfluidics: a new Cosset for Neurobiology," Lab Chip, **9**(5), pp. 644–652, doi: 10.1039/b813495b

[5] Pearce, T. M., and Williams, J. C., 2007, "Microtechnology: meet Neurobiology," Lab Chip, **7**(1), pp. 30–40, doi: 10.1039/b612856b

[6] Ben-Yakar, A., Chronis, N., and Lu, H., 2009, "Microfluidics for the Analysis of Behavior, Nerve Regeneration, and Neural Cell Biology in C. elegans," Curr. Opin. Neurobiol., **19**(5), pp. 561–567, doi: 10.1016/j.conb.2009.10.010

[7] San-Miguel, A., and Lu, H., 2013, "Microfluidics as a tool for C. elegans Research", *WormBook*, **24**, doi/10.1895/wormbook.1.162.1

[8] McDonald, J. C., and Whitesides, G. M., 2002, "Poly(dimethylsiloxane) as a Material for Fabricating Microfluidic Devices," Acc. Chem. Res., **35**(7), pp. 491–499, doi: 10.1021/ar010110q

[9] Xia, Y., and Whitesides, G. M., 1998, "Soft Lithography," Annu. Rev. Mater. Sci., **28**(1), pp. 153–184

[10] Chiu, D. T., Jeon, N. L., Huang, S., Kane, R. S., Wargo, C. J., Choi, I. S., Ingber, D. E., and Whitesides, G. M., 2000, "Patterned Deposition of Cells and Proteins onto Surfaces by using Three-dimensional Microfluidic Systems," Proc. Natl. Acad. Sci., **97**(6), pp. 2408–2413, doi: 10.1073/pnas.040562297

[11] Anderson, J. R., Chiu, D. T., Jackman, R. J., Cherniavskaya, O., McDonald, J. C., Wu. H., Whitesides, S. H., and Whitesides, G. M., 2000 "Fabrication of Topologically Complex Three-dimensional Microfluidic Systems in PDMS by Rapid Prototyping," Anal. Chem., **72**(14), pp. 3158–3164, doi: 10.1021/ac9912294

[12] Jo, B., Van Lerberghe, L. M., Motsegood, K. M., and Beebe, D. J., 2000, "Three-dimensional Micro-channel Fabrication in Polydimethylsiloxane (PDMS) Elastomer," J. Microelectromech. Syst., **9**(1), pp. 76–81

[13] Luo, Y., and Zare, R. N., 2008, "Perforated Membrane Method for Fabricating Three-dimensional Polydimethylsiloxane Microfluidic Devices," Lab Chip, **8**(10), pp. 1688–1694, doi: 10.1039/b807751g

[14] Liu, M., Sun, J., Sun, Y., Bock, C., and Chen, Q., 2009, "Thickness-dependent Mechanical Properties of Polydimethylsiloxane Membranes," J. Micromech. Microeng., **19**(3), p. 035028, doi: 10.1088/0960-1317/19/3/035028

[15] Kang, J. H., Um, E., and Park, J., 2009, "Fabrication of a Poly(dimethylsiloxane) Membrane with Well-defined Through-holes for Three-dimensional Microfluidic Networks," J. Micromech. Microeng., **19**(4), p. 045027, doi: 10.1088/0960-1317/19/4/045027

[16] Thangawng, A. L., Swartz, M. A., Glucksberg, M. R., and Ruoff, R. S., 2007, "Bond–Detach Lithography: A Method for Micro/Nanolithography by Precision PDMS Patterning," Small, **3**(1), pp. 132–138, doi: 10.1002/smll.200500418

[17] Armbruster, C., and Schneider, M., 2009, "Fabrication of Thin and Flexible PDMS Membranes for Biomechanical Test Applications," IFMBE Proceedings, **22**, pp. 2007–2010

[18] Thangawng, A. L., Ruoff, R. S., Swartz, M. A., and Glucksberg, M. R., 2007, "An Ultra-thin PDMS Membrane as a Bio/Micro-nano Interface: Fabrication and Characterization," Biomed. Microdevices, **9**(4), pp. 587–595, doi: 10.1007/s10544-007-9070-6

[19] Tong, J., Simmons, C. A., and Sun, Y., 2008, "Precision Patterning of PDMS Membranes and Applications," J. Micromech. Microeng., **18**(3), p. 037004, doi:

10.1088/0960-1317/18/3/037004

[20] Oh, K., and Chong, H. A., 2006, "A Review of Microvalves," J. Micromech. Microeng., **16**, doi: 10.1088/0960-1317/16/5/R01

[21] Takao, H., Miyamura, K., Ebi, H., Ashiki, M., Sawada, K., and Ishida, M., 2005, "A MEMS Microvalve with PDMS Diaphragm and Two-chamber Configuration of Thermo-pneumatic Actuator for Integrated Blood Test System on Silicon," Sens. Actuators, A, **119**(2), pp. 468–475, doi: 10.1016/j.sna.2004.10.023

[22] Liu, R. H., Yu, Q., and Beebe, D. J., 2002, "Fabrication and Characterization of Hydrogel-based Microvalves," J. Microelectromech. Sys., **11**(1), pp. 45–53

[23] Grover, W. H., Skelley, A. M., Liu, C. N., Lagally, E. T., and Mathies, R. A., 2003, "Monolithic Membrane Valves and Diaphragm Pumps for Practical Large-scale Integration into Glass Microfluidic Devices," Sens. Actuators, B, **89**(3), pp. 315–323, doi: 10.1016/S0925-4005(02)00468-9

[24] Jeong, O. C., 2005, "Fabrication of all PDMS Micro Pump" IEEE Int. Symp. Micro-NanoMechatronics Hum. Sci., pp. 139–143, doi: 10.1109/MHS.2005.1589977

[25] Lee, J. N., Park, C., and Whitesides, G. M., 2003, "Solvent Compatibility of Poly(dimethylsiloxane)-based Microfluidic Devices," Anal. Chem., **75**(23), pp. 6544–6554, doi: 10.1021/ac0346712

[26] Gevers, L. E. M., Vankelecom, I. F. J., and Jacobs, P. A., 2006, "Solvent-resistant Nanofiltration with Filled Polydimethylsiloxane (PDMS) Membranes," J. Membr. Sci., **278**(1–2), pp. 199–204, doi: 10.1016/j.memsci.2005.10.056

[27] Zhang, Y., Reed, J. C., and Yang, S., 2009, "Creating a Library of Complex Metallic Nanostructures via Harnessing Pattern Transformation of a Single PDMS Membrane," ACS Nano, **3**(80), pp. 2412–2418, doi: 10.1021/nn900650n

[28] Rosset, S., Niklaus, M., Dubois, P., and Shea, H. R., 2009, "Metal Ion Implantation for the Fabrication of Stretchable Electrodes on Elastomers," Adv. Funct. Mater., **19**(3), pp. 470–478, doi: 10.1002/adfm.200801218

[29] Schneider, F., Draheim, J., Müller, C., and Wallrabe, U., 2009, "Optimization of an Adaptive PDMS-membrane Lens with an Integrated Actuator," Sens. Actuators, A, **154**(2), pp. 316–321, doi: 10.1016/j.sna.2008.07.006

[30] Werber, A., and Zappe, H., 2008, "Tunable Pneumatic Microoptics," J. Microelectromech. Syst., **17**(5), pp. 1218–1227, doi: 10.1109/JMEMS.2008.928712

[31] Hongbin, Y., Guangya, Z., Siong, C. F., and Feiwen, L., 2008, "Simple Method for Fabricating Solid Microlenses With Different Focal Lengths," IEEE Photonics Technol. Lett., **20**(19), pp. 1624–1626, doi: 10.1109/LPT.2008.2002728

[32] Fieremans, E., Deene, Y. D., Delputte, S., Ozdemir, M. S., Achten, E., and Lemahieu, I., 2008, "The Design of Anisotropic Diffusion Phantoms for the Validation of Diffusion Weighted Magnetic Resonance Imaging," Phys. Med. Biol., **53**(19), pp. 5405–5419, doi: 10.1088/0031-9155/53/19/009

[33] Tournier, J., Yeh, C., Calamante, F., Cho, K., Connelly, A., and Lin, C., 2008, "Resolving Crossing Fibres using Constrained Spherical Deconvolution: Validation using Diffusion-weighted Imaging Phantom Data," Neuroimage, **42**(2), pp. 617–625, doi: 10.1016/j.neuroimage.2008.05.002

[34] Gulani V., and Sundgren, P. C., 2006, "Diffusion Tensor Magnetic Resonance Imaging," J. Neuro-Ophthalmol., **26**(1), pp. 51–60

[35] Samuel, R., Sant, H. J., Jiao, F., Johnson, C. R., and Gale, B. K., 2011, "Microfluidic Laminate-based Phantom for Diffusion Tensor-Magnetic Resonance Imaging," J. Micromech. Microeng., **21**(9), p. 095027, doi: 10.1088/0960-1317/21/9/095027

[36] Ebrahimi, B., Swanson, S. D., and Chupp, T., 2010, "A Microfabricated Phantom for Quantitative MR Perfusion Measurements: Validation of Singular Value Decomposition Deconvolution Method," IEEE Trans. on Biomed. Eng., **57**(11), pp. 2730–2736, doi:10.1109/TBME.2010.2055866

[37] Alexander, L. A., Lee, J. E., Lazar, M., and Field, A. S., 2007 "Diffusion Tensor imaging of the Brain," Neurotherapeutics, **4**(3), pp. 316–329, doi: 10.1016/j.nurt.2007.05.011

[38] Tanaka, K., 1975, "Measurements of Self-diffusion Coefficients of Water in Pure Water and in Aqueous Electrolyte Solutions," J. Chem. Soc., Faraday Trans. 1, **71**, pp. 1127–1131, doi: 10.1039/F19757101127

[39] Au, A. K., Lai, H., Utela, B. R., and Folch, A., 2011, "Microvalves and Micropumps for BioMEMS," Micromachines, **2**, pp. 179–220, doi: 10.3390/mi2020179

[40] Bartholomeusz, D., Boutte R. W., and Andrade J. D., 2005, "Xurography: Rapid Prototyping of Microstructures using a Cutting Plotter," J. Microelectromech. Sys., **14**(6), pp. 1364–1374, doi: 10.1109/JMEMS.2005.859087

[41] Kaigala, G. V., Ho, S., Penterman, R., and Backhouse, C. J., 2007, "Rapid Prototyping of Microfluidic Devices with a Wax Printer," Lab Chip, **7**(3), pp.

384–387, doi: 10.1039/b617764f

[42] Li, C., Cheung, C. N., Yang, J., Tzang, C. H., and Yang, M., 2003, "PDMS-based Microfluidic Device with Multi-height Structures Fabricated by Single-step Photolithography using Printed Circuit Board as Masters," Analyst, **128**(9), p. 1137, doi: 10.1039/b304354a

[43] Luo, L. W., Teo, C. Y., Ong, W. L., Tang, K. C., Cheow, L. F., and Yobas, L., 2007, "Rapid Prototyping of Microfluidic Systems using a Laser-patterned Tape," J. Micromech. Microeng., **17**(12), pp. N107–N111, doi: 10.1088/0960-1317/17/12/N02

[44] Waldbaur, A., Rapp, H., Länge, K., and Rapp, B. E., 2011, "Let there be Chip—towards Rapid Prototyping of Microfluidic Devices: One-step Manufacturing Processes," Anal. Methods, **3**(12), p. 2681, doi: 10.1039/clay05253e

[45] Morarka, A., Agrawal, S., Kale, S., Kale, A., Ogale, S., Paknikar, K., and Bodas, D., 2011, "Quantum Dot Based Immunosensor using 3D Circular Microchannels Fabricated in PDMS," Biosens. Bioelectron., **26**(6), pp. 3050–3053, doi: 10.1016/j.bios.2010.12.017

[46] McDonald, J. C., Chabinyc, M. L., Metallo, S. J., Anderson, J. R., Stroock, A. D., and Whitesides, G. M., 2002, "Prototyping of Microfluidic Devices in Poly (dimethylsiloxane) using Solid-object Printing," Anal. Chem., **74**(7), pp. 1537–1545, doi: 10.1021/ac010938q

[47] Asthana, A., Kim, K., Perumal, J., Kim, D., and Kim, D., 2009, "Facile Single Step Fabrication of Microchannels with Varying Size," Lab Chip, **9**(8), pp. 1138–1142, doi: 10.1039/b818987k

[48] Malek, C. G. K., 2006, "Laser Processing for Bio-microfluidics Applications (Part II)," Anal. Bioanal. Chem., **385**(8), pp. 1362–1369, doi: 10.1007/s00216-006-0517-z

[49] Huang, H., and Guo, Z., 2009, "Ultra-short Pulsed Laser PDMS Thin-layer Separation and Micro-fabrication," J. Micromech. Microeng., **19**(5), p. 055007, doi: 10.1088/0960-1317/19/5/055007

[50] Lieschke, G. J., and Currie, P. D., 2007, "Animal Models of Human Disease: Zebrafish Swim into View," Nat. Rev. Genetics, **8**(5), pp. 353–367, doi: 10.1038/nrg2091

CHAPTER 2

MICROFLUIDIC LAMINATE-BASED PHANTOM FOR DIFFUSION TENSOR-MAGNETIC RESONANCE IMAGING (DT-MRI)

Reprinted from Journal of Micromechanics and Microengineering, 2011, 21(9), p. 095027, doi: 10.1088/0960-1317/21/9/095027 (http://iopscience.iop.org/0960-1317/21/9/095027),

IOP Publishing Journal of Micromechanics and Microengineering
J. Micromech. Microeng. 21 (2011) 095027 (11pp) doi:10.1088/0960-1317/21/9/095027

Microfluidic laminate-based phantom for diffusion tensor-magnetic resonance imaging

R Samuel[1,3], H J Sant[1], F Jiao[2], C R Johnson[2] and B K Gale[1]

[1] State of Utah Center of Excellence for Biomedical Microfluidics, University of Utah, 50 S Central Campus Dr., Rm 2110, Salt Lake City, UT 84112, USA
[2] Scientific Computing and Imaging Institute, University of Utah, 72 S Central Campus Dr. Rm 3750, Salt Lake City, UT 84112, USA

E-mail: raheel.samuel@utah.edu, himanshu.sant@utah.edu, bruce.gale@utah.edu, fjiao@sci.utah.edu and crj@sci.utah.edu

Received 15 April 2011, in final form 5 July 2011
Published 19 August 2011
Online at stacks.iop.org/JMM/21/095027

Abstract
This paper reports fabrication of a magnetic resonance imaging (MRI) phantom created by stacking of multiple thin polydimethylsiloxane (PDMS) layers. PDMS is spin-coated on SU-8 molds to obtain the desired layer thickness and imprints of the microchannel patterns that define the phantom geometry. This paper also identifies the unique challenges related to the fabrication and assembly of multiple thin layers and reports for the first time assembly of a large number of thin laminates of this nature. Use of photolithography techniques allows us to create a wide range of phantom geometries. The target dimensions of the phantoms reported here are two distinct stacks of 30 thin PDMS layers each of 10 μm thickness with either (i) curved 5 μm $\times$ 5 μm microchannels with 8.7 μm spacing, or (ii) straight 5 μm $\times$ 5 μm microchannels with 3.6 μm spacing. SEM scans of the assembled phantoms show open microchannels and a monolithic cross section with no visible interface between PDMS layers. Based on the results of diffusion tensor magnetic resonance imaging scanning, the anisotropic diffusion of water molecules due to the physical restriction of the microchannels was detected, which means that the phantom can be used to calibrate and optimize MRI instrumentation.

(Some figures in this article are in colour only in the electronic version)

1. Introduction

Molecular diffusion refers to the random movement of molecules through space, driven by their internal thermal energy. It is a process that is highly sensitive to the physical structure of the microscopic environment. Diffusion tensor magnetic resonance imaging (DT-MRI) has been used to measure the diffusivity of water and metabolites noninvasively at microscopic length scales [1, 2]. DT-MRI measures the restricted random Brownian motion of water molecules [3]. During the MRI measurement interval (ms), the water molecule can diffuse a distance of 5–20 μm, while the diffusion tensor at each voxel measures the local diffusion profile. For the standardization of DT-MRI machines, standard physical models (also known as phantoms) are required with well-defined microscopic architecture. A proposed design for an MRI phantom is shown in figure 1. Artificial fiber diffusion phantoms have been fabricated using hemp, linen, polyamide, polyester, polyethylene and rayon [1]. However, it is important to develop artificial phantoms that can be reproduced in order to produce a particular MRI scan result, which will help in efforts for the validation of MRI technology. The quality of a phantom is typically dependent on the anisotropy of water diffusion (restricted random Brownian motion of water molecules) and the amount of water in the phantom, which in turn determines the phantom design. The size of the PDMS-based phantom developed in this work was 1.5 cm $\times$ 1.5 cm $\times$ 0.3 mm to obtain an image of about 15 $\times$ 15 voxels of 0.5 mm or 1 mm cubes.

[3] Author to whom any correspondence should be addressed.

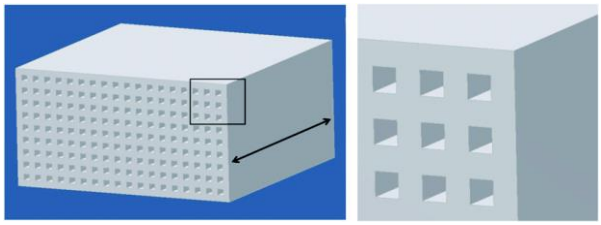

Figure 1. Left: a 3D schematic of the envisioned multilayer phantom (not to scale), the targeted dimensions are height: 0.3 mm, width: 1.5 cm, length: 1.5 cm. Each layer is 10 μm thick with 5 μm × 5 μm channels. Spacing between channels (3.6 or 8.7 μm) and the orientation (curved channels or straight channels) is varied for each phantom. The diffusional direction of water molecules is shown by the double-headed arrow. Right: a magnified view of the cross-sectional area marked by a black square in the left picture (small microchannels can be observed). With microfabrication techniques, we can reproduce such highly parallel, multilayered microchannels consistently.

PDMS is a popular material for biomedical applications because of its outstanding material properties and the simplicity with which it can be cast onto microstructured molds [4]. Most PDMS-based microfabricated products require micromolding of microchannels in PDMS layers and later bonding of these layers to glass/silicon or to another PDMS surface for the realization of the final product. Currently, soft lithography-based PDMS layer fabrication uses two approaches: spin-casting or the membrane-sandwich method [5, 6]. However, PDMS has its own microfabrication challenges. Peeling off a freely suspended spin-cast, ~10 μm thick PDMS layer, from a molding substrate such as a silicon wafer is a significant challenge. Such thin layers are very delicate and once torn are easily damaged during the peeling process [7]. However, in some cases PDMS layers as thin as 70 nm and without embedded structures have been spun-cast and later peeled off. Demolding these layers requires the presence of an adhesion reduction layer between PDMS and the silicon substrate [8]. There are further hurdles in stacking these ultra-thin, spin-coated layers—the occurrence of air bubbles and wrinkles. However, researchers have been able to efficiently stack five relatively thick (120 μm) PDMS layers for 3D microfluidic channel realization by using the membrane-sandwich method [6], and a variation of the same method was used to assemble six (50 μm thick) layers [9]. In the membrane-sandwich method, uncured PDMS is placed between a SU-8 mold and a flat rigid plate. The flat rigid plate is pressurized from the top, which in turn squeezes the PDMS in between the mold and plate. Different layer thickness can be achieved by varying the applied pressure. After applying the required pressure, the whole assembly is heated and the PDMS layer cures, which is then peeled off the mold. The membrane-sandwich method [5, 6] allows great control in the fabrication process [10] but is limited to relatively thick and mechanically weaker layers (>20 μm) [11].

The geometry of the phantoms described in this paper was determined by the requirement of high MRI signal to noise ratio. During MRI scanning, high signal to noise ratios can be achieved if the phantoms can retain large amounts of water (i.e. a high ratio of combined microchannel volume/phantom volume) and high diffusion anisotropy. Consequently, each phantom layer necessitated a dense array of parallel microchannels and the layers needed to be as thin as could be handled easily and manufactured with high reproducibility. Based on these design criteria, the thickness of the PDMS layers was set to 10 μm. Fabricating a 10 μm thick layer with thousands of 5 μm × 5 μm (approximately) patterned parallel microchannels in an area of 1.5 mm × 1.5 mm is more feasible when they are spin-cast on SU-8 molds in standard photoresist spinners (available in almost all microfabrication labs) than with the previously mentioned membrane-sandwich methods (with reference to their relatively large microchannel dimensions, larger layer thickness and low microchannel density per layer) [6, 9]. Another variation of the membrane-sandwich approach used by Zhang *et al* [9] for thin PDMS layer stacking is the use of fluorosilanes for selective transfer of the PDMS microstructure from mold to final assembly with an intermediate transfer step [9]. Success of such an approach remains to be investigated when very thin PDMS layers (<20 μm) for a dense network of molded microchannels need to be assembled. In contrast, our approach utilizes spin-cast PDMS layers that are mechanically stronger than standard casting as the stretching of polymer chains in the radial direction on spinning at high spin speeds improves mechanical strength significantly [11]. This helps in proper release of the highly patterned layer from the mold, without any damage and permanent deformation of the layer. However, stacking a large number (~30) of thin (<20 μm) spin-cast patterned PDMS layers has so far not been demonstrated in the literature.

This work reports a unique fabrication process for fabricating patterned 10 μm thick PDMS layers cast from a standard SU-8 soft lithographic mold into a 30-layer laminate. Each layer includes thousands of microchannels that are filled with deionized (DI) water. The layers are created using conventional spin-casting techniques on a large mold area and later stacked and bonded by a repeatable and uniform stacking method. The unique feature of this method is the use of a thick transfer ring, made from PDMS as well to transport and assemble the thin PDMS layers while allowing the use of a unique air-pressure technique to bond stacked layers activated by a corona discharge. This special air-pressure technique helps in stacking the layers without any trapped air bubbles or wrinkles. When the 30 layers are stacked, they are immersed in DI water and then sealed in a PDMS block before being used

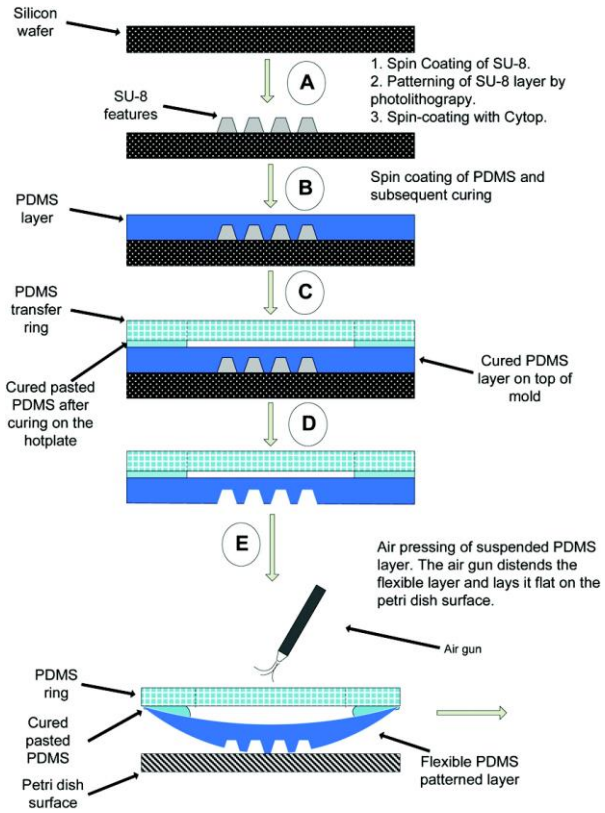

Figure 2. A schematic diagram of the phantom fabrication showing the PDMS softlithography steps, the use of the SU-8 mold and the transfer ring for the assembly of thin PDMS layers.

as a MRI phantom. By taking MR images of this phantom, researchers will be able to improve imaging characteristics of MRI machines.

2. Methods

The fabrication process used in this work is simple but can be best explained using three separate illustrations (figures 2–4), with the main steps designated in order and identified with a step number from A–M which is referred to in the description of the relevant process step.

2.1. SU-8 mold fabrication and pretreatment (step A, figure 2)

The individual patterned microfluidic laminates were created using SU-8 micromolding and PDMS soft lithography techniques in a normal room environment on a 4 inch silicon wafer (Silicon Qwest International Inc., Santa Clara, CA).

SU-8 2005 (Micro Chem, Newton, MA) was spun on the silicon wafer at 2500 rpm for 30 s at a ramp of 300 rpm s^{-1} and soft baked at 95 °C for 2 min on a leveled hot plate. The phantoms were fabricated using two mask patterns. One mask pattern generated a SU-8 mold with curved 5 μm wide channels with 8.7 μm channel spacing. The other mask pattern generated straight 5 μm wide channels with 3.6 μm channel spacing. An exposure bandpass filter (PL-360 LP, Omega Optical, Brattleboro, VT) was used to allow transmission of 365 nm wavelength light. A dose of 100 mJ cm^{-2} was used to expose ~5 μm thin SU-8 through the appropriate mask. The exposure time was set to 9 s on a mask aligner (EV-420, EV Group Inc. Tempe, AZ). After exposure, the substrate was post-baked for 3 min at 95 °C and later developed in the SU-8 developer for 2 min followed by isopropanol rinsing and drying with nitrogen gas. The patterned wafer was hard baked on a hotplate at 150 °C for 2 min.

Prior to micromolding the PDMS, the SU-8 mold was coated with a thin layer (~ 400 nm) of Cytop (CTL-809M,

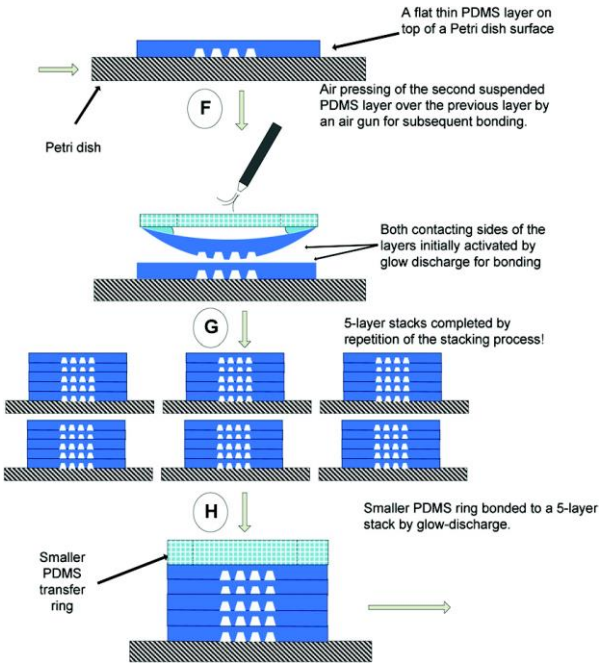

Figure 3. Summary of the fabrication process, depicting stacking of 30 layers to make six separate five-layer stacks. This approach improves the yield as any error during fabrication is limited to smaller stacks.

Asahi Glass Co. Ltd, Ibaraki, Japan). Cytop acts as an adhesion reduction layer between PDMS and silicon [8]. After the SU-8 hard bake, Cytop was spin-coated at 5000 rpm for 1 min with a 300 rpm s^{-1} ramp and cured at 180 °C on a leveled hotplate for 1 h.

2.2. PDMS molding (step B, figure 2)

Once the SU-8 mold was completed, the next step was to cast the PDMS layers on the mold. All the PDMS (Slygard® 184 Silicone Elastomer, Dow Corning, MI) used in this paper had the PDMS base to curing agent ratio of 5:1.

For layer fabrication, uncured PDMS was spun on the SU-8 mold with the overlying Cytop layer at 5000 rpm for 1 min (∼10 μm thick) (step B). The layer was cured at 100 °C for 10 min on a hot plate with an aluminum foil-cover to minimize foreign particulate contamination.

2.3. PDMS layer picking and assembly (steps C and D, figure 2)

At ∼10 μm, PDMS spin-cast layers have significant stress and are difficult to handle and tend to fold onto themselves. One of the challenges in this work was to remove such thin PDMS layers off the 4 inch SU-8 mold (large surface area) without damaging the very small molded microchannels on the layer or the layer itself or any of the microstructures across the substrate. To facilitate easy removal of the thin PDMS layer, a 3 mm thick transfer ring was made which had an outer diameter of 135 mm and inner diameter of 68 mm. The transfer ring was used as a holder that bonds the ends of the PDMS layer to lift the thin layer. Furthermore, the transfer ring provided a mechanical support to the thin layer after peeling it off from the mold. The ring was made using the standard PDMS casting process to make a PDMS slab and then a razor was used to core out the ring-shaped PDMS. In preparation for picking up the thin layers, uncured PDMS was applied using a spatula to the ends of the PDMS layer overlying the SU-8 mold. The uncured PDMS was applied such that it formed a ring on the overlying PDMS layer. This ring of uncured PDMS had an outer diameter the same as that of the mold (100 mm) and inner diameter of approximately 75 mm. In this way, the uncured PDMS did not interfere with the patterned microstructures (in the center of the layer) on the thin PDMS layer, overlying on the SU-8 mold. The transfer ring was placed on the mold such that it made a good contact with the uncured PDMS (step C). Both the mold and transfer ring on top of the PDMS were placed on a hotplate at 100 °C for 5 min. This process resulted in adhesion of the thin layer to the transfer ring. For PDMS layer removal, the transfer ring was first gently separated from

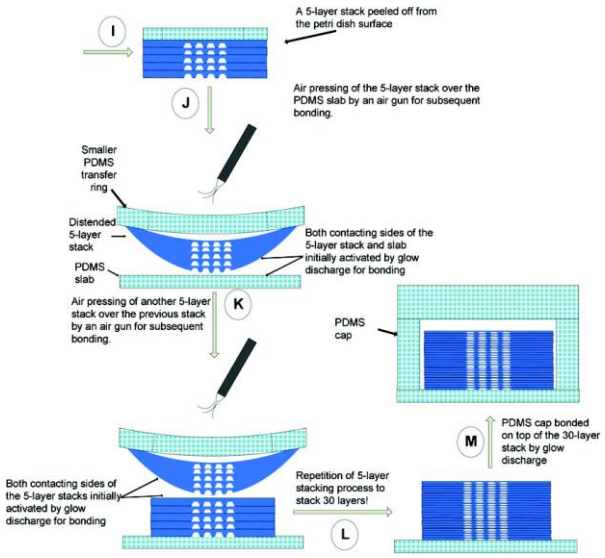

Figure 4. Summary of the fabrication process, depicting stacking of six five-layer stacks to make a single 30-layer stack and encasement of the stack by a PDMS cap for the realization of the final product.

the mold's edges. The transfer ring was then slowly pulled up from the mold from one end to the other, and the thin PDMS layer was brought with it, ensuring peeling off the thin PDMS layer without tearing (step D).

2.4. Stacking of the layers (step E, figure 2; steps F–H, figure 3; steps I–L, figure 4)

Each molded layer had up to 16 distinct phantom designs on it. A single microfluidic phantom was a 30 layer-laminate of only one of these 16 distinct designs (we used two of these designs to make two distinct microfluidic phantoms mentioned in this paper).

The main challenge of this work was the stacking of large number of highly flexible thin PDMS layers (at least 30 layers, to reach the minimum stack height for the MRI scanner used in this study), without the presence of any trapped air bubbles, wrinkles and delamination of the bonded layers. The stacking methodology had to be simple enough to be carried outside the clean room without the use of any complicated hardware, so as to be cost effective.

A Petri dish (Part 0875713, Fisher Scientific, Pittsburgh, PA) was used as the base while stacking the layers, as the polystyrene Petri dishes have low adhesion between Petri dish surface and cured PDMS, which provides an easy removal of the stacked PDMS laminates. After peeling off the PDMS layer from the mold, it was placed on a Petri dish gently by using air pressure to lay it flat (step E). Care was taken to make sure that no air bubbles formed between the PDMS layer and the Petri dish. Wrinkles and bubbles were avoided by bringing one end of the suspended layer in contact with the Petri dish surface and pressing it flat with air pressure (using a low-pressure compressed-air nozzle), starting from one end and progressively moving to the other end. The PDMS layer was separated from the transfer ring with a knife cut to release the transfer ring. There was enough room for the knife cut, so as to avoid any permanent damage to the molded structures located near the center of the wafer. For addition of the second layer, both mating surfaces were activated with a corona/glow discharge (LM4243-05, Enercon Industries Corporation, WI). The second layer was gently placed on top of the first layer using the same air-pressure technique and knife cut as described earlier (step F). No special hardware was used for layer alignment and was done by the naked eye using phantom borders as alignment marks. The same procedure was repeated to assemble six separate five-layer stacks (step G). The phantom design for this study required a stack of 30 thin layers of PDMS microstructures. For optimal phantom performance, each layer had to be flat without any wrinkles, trapped air bubbles or any layer detachment. For efficient layer stacking and consistent fabrication yield, six separate stacks of five layers each were fabricated and then stacked on each other to make a single 30-layer stack.

To facilitate the handling of five-layer stacks, a smaller PDMS transfer ring was used. Corona (glow discharge) treatment was done on top of one of the five-layer stacks to be used as a base stack on which other five-layer stacks would be stacked. One side of the smaller transfer ring was also activated by corona discharge and that face was placed on top of the base stack and pressed for 2 min before peeling off

the base stack from the Petri dish (steps H and I). The bottom surface of the base stack which was previously in contact with the Petri dish was activated with corona and placed on top of a cured and corona-treated PDMS substrate of 10 mm thickness (step J). The base stack was laid flat on the PDMS substrate using the same compressed air-pressure technique as was described earlier and cut free from the transfer ring with a sharp knife. The entire assembly procedure was repeated until a phantom prototype with 30 layers was created (steps K and L).

2.5. Device testing

To ensure that the microchannels had not collapsed and were filled with DI water, scanning electron microscope (SEM) scans of a phantom model's (five-layer stack) cross section after immersing it in a pool of polystyrene beads and DI water were collected. The purpose was to fill the microchannels with water, which will carry the polystyrene particles along with it. When the water is evaporated, the entrained polystyrene particles can be detected by imaging the cross section (approximately mid-way across the length of the channels) of the five-layer stack, which will confirm that the channels are being filled with DI water.

To accomplish the filling of the phantom with water, the phantom model was placed in a Petri dish. The Petri dish was filled with DI water containing 10% (by volume) polystyrene microspheres of 0.202 μm diameter (Part 07304, Polysciences Inc., PA). The Petri dish was placed in a vacuum chamber at moderate vacuum (–26 inHg) for 2 min, which degassed the microchannels and filled them with water. The stack was washed with DI water and dried in an oven at 62 °C for 2 h. Later, the stack was cut in the middle, across the channels by a fine blade. The newly exposed cross section was imaged by a SEM.

2.6. Device assembly (step M, figure 4)

The 30 layers laminated in the end of step L in figure 4 were pressed flat by a small roller to ensure that all the layers were evenly bonded and no layer delamination occurred. The microchannels of the phantom prototypes were opened by cutting the edges of the channels with a fine blade. The entire phantom was sealed using a PDMS cap that was corona-bonded to the PDMS substrate (step M). The PDMS cap also outlined a reservoir area around the phantom that contained DI water. A 2 mm thick PMMA (Polymethyl methacrylate) sheet (25 mm × 25 mm) was bonded with double-sided tape in a polystyrene Petri dish, to make a mold for the PDMS cap. The entire phantom assembly was cured overnight in an oven at 65 °C to improve the bond strength between different layers of phantom and ensure a leak-proof seal between the PDMS substrate and the cap. After cooling of the phantom prototype, DI water was injected through the PDMS cap using a syringe with a 27G needle until the reservoir containing the phantom was completely filled. The holes made by the syringe needle were sealed using a silicone elastomer (734 Flowable Sealant, Dow Corning, MI) to prevent any DI water leaking out of the reservoir. The submerged phantom was placed in a vacuum chamber at moderate vacuum (-26 inHg) for 2 min to degas the microchannels and to ensure that they were completely filled with water.

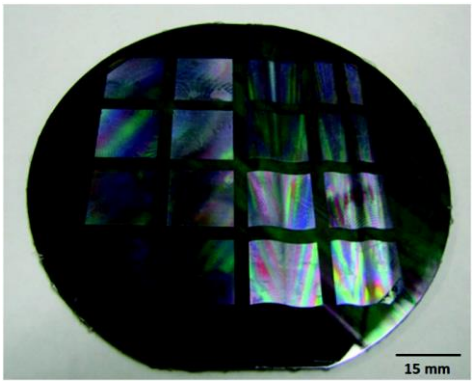

Figure 5. Photograph of the SU-8 mold with 16 distinct patterns, made using a 4 inch silicon wafer.

2.7. MRI imaging details

Imaging experiments of the MRI phantom were conducted on a Bruker Biospec 7 T horizontal-bore system (Bruker Inc, Billerica, MA) controlled by Paravision 5.0 software. For data acquisition, a standard 3D diffusion-weighted spin-echo sequence was used (in-plane resolution is 0.781 25 mm × 0.781 25 mm, and the slice thicknesses is 0.5 mm, diffusion-weighting b-value is 800 s mm^{-2}). For post-processing, diffusion tensors were computed on a voxel-by-voxel basis via weighted nonlinear least-squares fitting to extract the eigenvalues and their corresponding eigenvectors of the tensor matrix. The eigenvalues and eigenvectors correspond to the ensemble diffusivity and the ensemble diffusion directions of the local water molecules correspondingly.

3. Results and discussions

3.1. SU-8 mold fabrication

Figure 5 shows the SU-8 mold on a 4″ silicon wafer. This mold contained 16 distinct phantom designs on a 15 mm × 15 mm footprint. Exposure of the micropatterns was done such that the phantom of interest was placed at the center of the wafer. The patterns produced by the mold were found to be reproducible and meet the target width and spacing of the microstructures. Figure 6 shows an SEM scan of the cross section of the SU-8 mold used for phantom fabrication. The mold was diced in two by a wafer-dicing machine (DAD 641, DISCO Corp., Tokyo, Japan) and the newly exposed cross section was imaged by a SEM. The channel wall height of the mold was measured from the SEM scan and found to be 4.00 μm for an SU-8 2005 spun at a spin speed of 2500 rpm for 30 s, with ∼ 400 nm overlying Cytop layer.

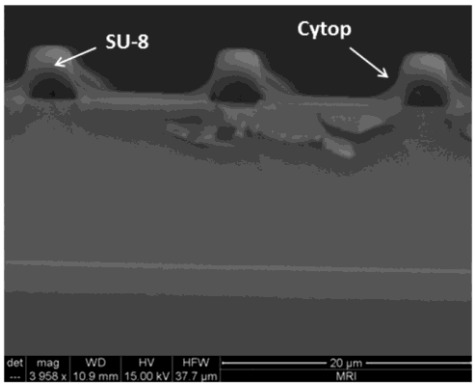

Figure 6. Picture showing SEM scan of the cross section of diced end of the SU-8 mold.

It should be noted that the same SU-8 mold was used to obtain all 30 layers for fabricating a microfluidic phantom. No damage or permanent deformation of the mold's microstructures was observed in the entire fabrication process of a single phantom.

3.2. PDMS molding: layer thickness and strength

In order to produce layers with precise thickness, the spinner was calibrated to achieve near-10 μm thick layers. Figure 7 shows a spin curve for PDMS spun on a 100-mm silicon wafer with a 400 nm overlying layer of Cytop. The thickness of each PDMS layer was measured by imaging the cross section of the layer under an optical microscope (Nikon Optiphot 88, Nikon Instruments Inc., Melville, NY). This method has been demonstrated to have reasonable accuracy (0.2%) for thin PDMS layer thickness measurements [12].

To determine the average thickness of each layer of the phantom, thicknesses of three individual five-layer stacks were measured at three distinct points. A total of nine data points were used to obtain an average individual layer thickness as 11.6 ± 0.5 μm.

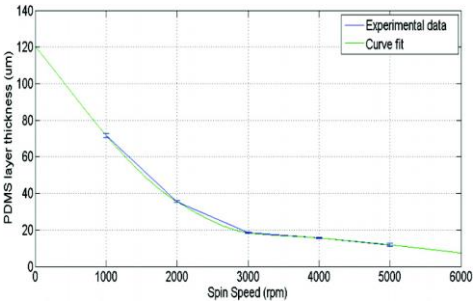

Figure 7. Plot of PDMS layer thickness (μm) versus spinner spin speed (RPM). The PDMS used for this work has the base to curing agent ratio of 5:1.

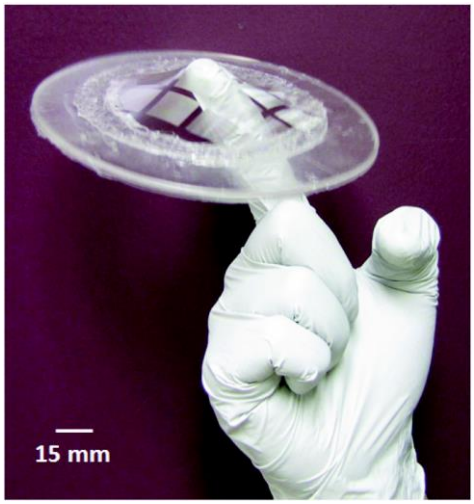

Figure 8. Picture of a PDMS transfer ring (weighing 30 g) being supported by ~10 μm thin membrane at the tip of a finger.

Interestingly, these thin PDMS membranes even with phantom microstructures proved to be very strong even at ~10 μm thickness. Figure 8 shows a picture of the PDMS layer attached to the transfer ring (weighing 30 g) being held at the center with the tip of a finger. This result is in accord with Liu *et al* [11] and very useful while picking up the layers and aligning them to fabricate a stack of multiple laminates.

3.3. PDMS layer picking and assembly

Figures 8 and 9 show the transfer ring that is used to pick up individual PDMS layers from the SU-8 mold. While some of the microstructures are lost because of the transfer ring overlay (figure 9), the single layer can be lifted off the mold cleanly without any effect to the layer structural integrity. In addition, this loss of microstructures due to the transfer ring overlay did not warrant any changes to the phantom design as the patterns in the center of the mold were of interest and used to fabricate all the phantoms we described in this paper. The *usable* phantom can be selected easily while aligning the mask to the SU-8 mold during exposure. However, the size of the uncured adhesive PDMS ring can be further optimized to provide the least overlay of the transfer ring onto the mold. Furthermore, a larger wafer can also be used to leave enough distance from the edge of the mold to achieve the same effect.

The PDMS ring was 3 mm thick. We found that a thicker PDMS ring would not be flexible enough to facilitate peeling off the thin layers, while a thinner ring would be too flexible to provide sufficient mechanical support to avoid folding of

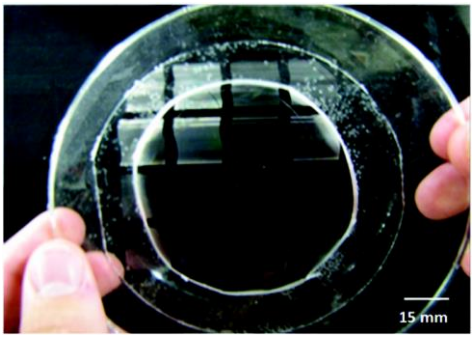

Figure 9. Picture of a PDMS transfer ring used to support and peel the thin layers of PDMS with microstructures. A supported PDMS layer with 16 distinct patterns (molded areas) can be seen in the picture.

the thin layer on itself. We were able to peel off at least 20 layers from a single PDMS ring before discarding it. After peeling off about 20 layers, the PDMS ring was not able to bond evenly to the thin layers and resulted in increased tearing of the thin layers during the peeling process. Bonding of the PDMS transfer ring to the thin PDMS layer on the SU-8 mold (shown in figure 5) was crucial for successful removal of the layer from the SU-8 mold. The bond had to be sufficiently strong and uniform at the ring and layer interface to overcome the stresses during peeling without tearing. We used two approaches to bond the PDMS ring to the PDMS layer overlying on the SU-8 mold: corona-discharge method and uncured PDMS as an adhesive. While the corona-discharge method was fast, it resulted in burnt PDMS particles on the thin layers (overlying the SU-8 mold) resulting in a damaged surface, which made the layer peeling very difficult. For this reason, a thin layer of uncured PDMS was used as an adhesive to bond the transfer ring to the thin layer on the SU-8 mold. Furthermore, different types of PDMS-to-PDMS bonding techniques have been evaluated for their bond strengths and using uncured PDMS as an adhesive for bonding has been shown to have the highest bond strength [13].

3.4. Stacking of the layers

The thin PDMS layers (containing microchannels) needed to be stacked with the least axial misalignment. The stacking in this case was done with the naked eye (with phantom borders as alignment marks) and may have some minor axial misalignments, but these misalignments can be reduced by stacking under a microscope or by utilizing an aligner specially designed to align PDMS layers [14]. The angular alignment of the microchannels along the length is very important for this application such that all the channels should point in the same direction to achieve high resolution and accuracy of the MRI scan. In future, a PDMS aligner may be used for more accurate alignment.

Figure 10 shows SEM (Quanta 600 FEG, FEI, OR) scans of the phantom model composed of a five-layer stack. The channels have a smooth trapezoidal cross section. The trapezoidal cross section is due to the overlying 400 nm Cytop layer, which was spin-coated after the SU-8 mold was made by photolithography. While the trapezoidal cross section of the channels does not affect the phantom performance, a thinner passivation layer can be obtained using fluoropolymers (monolayer thickness) that can be deposited by chemical vapor deposition [15], ion-sputtering deposition [16] or vacuum deposition [17] and subsequent evaporation if needed. The effect of using such a deposition approach on PDMS thin layer peeling remains to be investigated. Nevertheless, the large aspect ratio (channel length to height) and not the microchannel profile ensures anisotropic diffusion, the key requirement for MRI phantoms. Figure 11 shows the SEM scan of a 16-layer stack (consistent bonding between each individual layer should be noted). Figure 11 clearly shows no delamination for a stack of 16 layers, an important achievement for successful phantom fabrication.

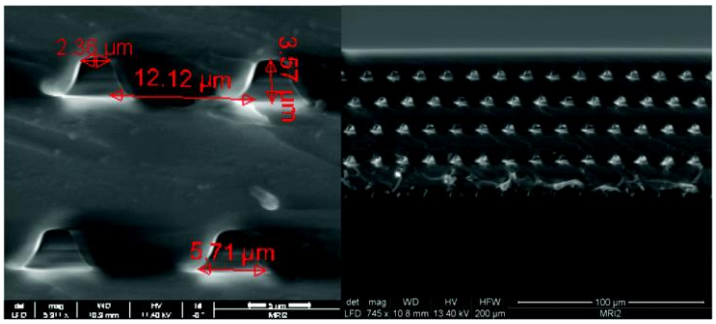

Figure 10. Image of a SEM scan of a five-layer stack of the PDMS layer showing the measured geometrical dimensions.

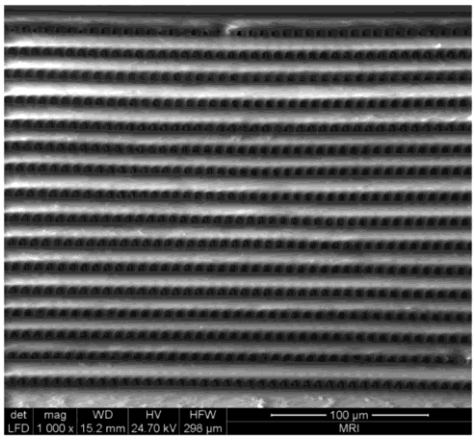

Figure 11. Image of a SEM scan of a 16-layer PDMS stack; the stack of layers after curing results in a monolithic structure with no visible interface separating the layers.

In figure 10, the height of the channels in the layers is 3.57 μm and about 0.43 μm smaller than the channel wall height (4.00 μm) in the mold. Possible reasons for this 0.43 μm difference are (i) shrinkage of PDMS on curing at a reasonably high temperature (100 °C) [18], (ii) relative stretching of the PDMS layer (during the bonding process) with respect to the previous bonded layer and (iii) variation in Cytop coating across the substrate. But such differences in channel parameters were allowable for this application. The layer channel height of 5 μm (if desired) can be obtained by varying the channel wall height in the mold to compensate for PDMS shrinkage and other effects. Furthermore, a Cytop layer of thickness less than 400 nm can be obtained by utilizing Cytop thinners available from Asahi Glass Co. Ltd, Japan.

3.5. Device testing

The newly exposed cross sections in the device testing (articulated in section 2.5) of the phantom were imaged by the SEM, and polystyrene particles were seen stuck on the inner microchannel walls in multiple scans (figure 12). This confirmed that the channels were being filled with DI

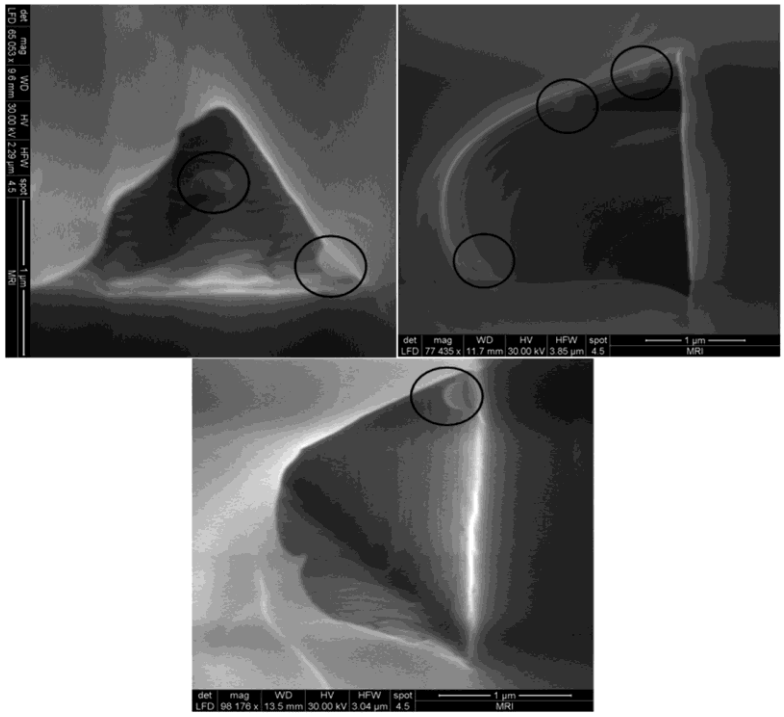

Figure 12. Images of SEM scans of microchannel cross sections showing polystyrene particles stuck on channel walls (particles marked by circles).

Figure 13. The pictures of two assembled MRI phantoms (left: with curved channels, right: with straight channels) along with a US quarter coin. Each phantom is placed in a square water reservoir formed by the PDMS cap and PDMS substrate. No air bubble can be seen in the phantom assembly.

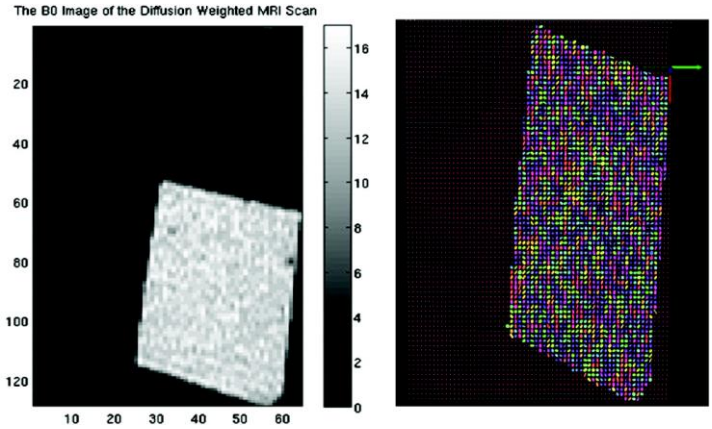

Figure 14. The B0 image (left-hand side) and the diffusion tensor image (right-hand side) of the phantom.

water and the polystyrene particles were carried inside the microchannels.

3.6. Device assembly

Figure 13 shows the fully fabricated MRI phantoms. The phantoms are immersed in a PDMS reservoir with DI water. The water infusion and air bubble withdrawal were done with 27 G non-coring needles attached to the plastic syringes.

3.7. Diffusion tensor imaging

Figure 14 shows the visualization of the B0 image (left) and the diffusion tensor image (right) of an MRI scan of the phantom shown in figure 13 (left). The diffusion tensor image's color variation depicts the alignment of the major eigenvector in different directions (x, y and z directions). From figure 14 (left), one can clearly see that the phantom was filled with water without any air bubbles (as the white area represents water and dark area represents absence of water). Based on figure 14 (right) the water molecule shows a certain degree of anisotropic diffusion. Due to the influence of the imaging background noise and possibly the misalignment between each stack, the anisotropy of each tensor is not as strong as expected. Additionally, the MRI instrumentation may not yet be able to adequately measure at these scales, so additional software development may be needed to better represent the movement of molecules in the phantom. Finally, the relative volume of water in the phantom may need to be increased to increase the signal available to the MRI instruments. Higher relative volumes of water would require higher aspect ratio channels with thicker layers, which is an ongoing effort.

4. Conclusion

A simple method of stacking patterned spin-coated ~10 μm thick PDMS layers with densely packed microstructures has been developed and demonstrated. The stacking of up to

30 such layers has been performed without the presence of any trapped air bubbles or wrinkles. The unique layer-stacking technique can be used to fabricate MRI diffusion phantoms as gold standards for MRI machines. Furthermore, the methods developed in this project can be used to fabricate 3D structures in thin spin-coated PDMS layers, leading to sophisticated microfluidic chips fabricated with automated aligners for higher precision. The stacked layers were easy to handle once assembled and microchannels retained their cross section as evidenced by SEM scans. Additionally, the methods shown in this work allow for the assembly of large areas of thin layers with dense networks of microstructures with high repeatability and reproducibility. While the MRI phantoms reported here were fabricated in a normal laboratory environment, even better fabrication results in terms of layer bonding can be predicted if fabrication is carried out in a clean room environment.

Overall, we have presented a 30-layer MRI phantom fabricated with microfluidic laminates for the first time. A high signal to noise ratio during phantom scanning requires high water diffusion anisotropy and high water content inside the phantom channels, a significant challenge. Optimal dimensions and arrangements for the MRI phantom still need to be developed to improve the function of the phantom, though the methods presented here provide sufficient function to begin optimization of MRI algorithms for imaging of small fluid structures.

Acknowledgments

This work was funded in part by the NIH NCRR Center for Integrative Biomedical Computing (www.sci.utah.edu/cibc), NIH NCRR grant no 5P41RR012553-11 and NIH grant S10 RR023017 for supporting the Small Animal Imaging Facility. The authors thank Brian Baker and the nanofabrication facilities at the University of Utah for their help with this project.

References

[1] Fieremans E, Deene Y D, Delputte S, Ozdemir M S, Achten E and Lemahieu I 2008 The design of anisotropic diffusion phantoms for the validation of diffusion weighted magnetic resonance imaging *Phys. Med. Biol.* **53** 5405–19

[2] Tournier J-D, Yeh C, Calamante F, Cho K, Connelly A and Lin C 2008 Resolving crossing fibres using constrained spherical deconvolution: validation using diffusion-weighted imaging phantom data *NeuroImage* **42** 617–25

[3] Basser P J, Mattiello J and Lebihan D 1994 Estimation of the effective self-diffusion tensor from the NMR spin echo *J. Magn. Reson.* B **103** 247–54

[4] McDonald J C and Whitesides G M 2002 Poly(dimethylsiloxane) as a material for fabricating microfluidic devices *Acc. Chem. Res.* **35** 491–9

[5] Chiu D T, Jeon N L, Huang S, Kane R S, Wargo C J, Choi I S, Ingber D E and Whitesides G M 1999 Patterned deposition of cells and proteins onto surfaces by using three-dimensional microfluidic systems *Proc. Natl Acad. Sci. USA* **97** 2408–13

[6] Jo B, Van Lerberghe L M, Motsegood K M and Beebe D J 2000 Three-dimensional micro-channel fabrication in PDMS elastomer *J. Microelectromech. Syst.* **9** 76–81

[7] Sarma S and Krishnan S 2009 A process for manufacturing very thin PDMS films *Transactions of NAMRI/SME* **37** 277–83

[8] Thangawng A L, Ruoff R S, Swartz M A and Glucksberg M R 2007 An ultra-thin PDMS membrane as a bio/micro–nano interface: fabrication and characterization *Biomed. Microdevices* **9** 587–95

[9] Zhang M, Wu J, Wang L, Kang X and Wen W 2010 A simple method for fabricating multi-layer PDMS structures for 3D microfluidic chips *Lab Chip* **10** 1199–203

[10] Moraes C, Sun Y and Simmons C A 2009 Solving the shrinkage-induced PDMS alignment registration issue in multilayer soft lithography *J. Micromech. Microeng.* **19** 065015

[11] Liu M, Sun J, Sun Y, Bock C and Chen Q 2009 Thickness-dependent mechanical properties of polydimethylsiloxane membranes *J. Micromech. Microeng.* **19** 035028

[12] Zhang W Y, Ferguson G S and Tatic-Lucic S 2004 Elastomer supported cold-welding for room temperature wafer level bonding *IEEE Conf. MEMS 2004 Technical Digest (Maastricht, the Netherlands)* pp 741–4

[13] Eddings M A, Johnson M A and Gale B K 2008 Determining the optimal PDMS-PDMS bonding technique for microfluidic devices *J. Micromech. Microeng.* **18** 1–4

[14] Kim J Y, Baek J Y, Lee K A and Lee S H 2005 Automatic aligning and bonding system of PDMS layer for the fabrication of 3D microfluidic channels *Sensors Actuators* A **119** 593–8

[15] Lee K, Bhushan B and Hansford D 2005 Nanotribological characterization of fluoropolymer thin films for biomedical micro/nanoelectromechanical systems applications *J. Vac. Sci. Technol.* A **23** 804–10

[16] Quaranta F and Valentini A 1993 Ion-beam sputtering deposition of fluoropolymer thin films *Appl. Phys. Lett.* **63** 10–1

[17] Chen J, Ko F, Hsieh K, Chou C and Chang F 2004 Effect of fluoroalkyl substituents on the reactions of alkylchlorosilanes with mold surfaces for nanoimprint lithography *J. Vac. Sci. Technol.* B **22** 3233–41

[18] Lee S W and Lee S S 2008 Shrinkage ratio of PDMS and its alignment method for the wafer level process *Microsyst. Technol.* **14** 205–8

CHAPTER 3

SIMPLE AND COST-EFFECTIVE MANUFACTURING OF MICROVALVE ARRAYS IN PDMS USING LASER CUT MOLDS WITH APPLICATION TO C. ELEGANS MANIPULATION IN MICROFLUIDICS

Abstract

This chapter presents a new fabrication protocol for fabricating pneumatically controlled microvalve arrays (consisting of 100s of microvalves) in PDMS substrates. The protocol utilizes rapid and cost-effective fabrication of molds using laser cutting of adhesive vinyl tapes (introduced here for the first time) and replica molding of PDMS. Hence the protocol is fast, simple, and avoids cleanroom use. The results show that effective doormat-style microvalves can be easily fabricated in arrays by manipulating the stiffness of the actuating membrane through varying the valve-chamber area/shape. Three frequently used valve-chamber shapes (circle, square, and capsule) were tested, and all showed advantages in different situations. Circular valve chambers were best for small valves; square valves were best for larger valves, and the capsule valves provided the easiest alignment. An application of this protocol has been demonstrated in the fabrication of a microfluidic 32-well plate for high-throughput manipulation of adult *C. elegans* for biomedical research.

Introduction

Microfluidics is rapidly becoming an important technology for the development of a variety of biomedical research tools [1]. A biomedical area of recent interest has been the development of microfluidic devices for processing *Caenorhabditis elegans* (*C. elegans*), a type of nematode or worm, for neuronal-behavior studies [2]. Neuroscience questions are the primary drivers for the use of *C. elegans*, and these organisms are used to understand the working of neural circuits and the influence of particular neurons on the behavior of multicellular organisms [3]. However, the small size of *C. elegans* is very inconvenient when manually handling/manipulating a large number of *C. elegans* during high-throughput screens, but these challenges are where microfluidics excels and can be of great benefit to worm biologists. In particular, microfluidics and *C. elegans* are a good match because of the small size of the worms (1.3-mm length and 80 μm in diameter for healthy adults) and the ability to use cellular imaging tools with microfluidics. In addition, because microfluidic manipulation of *C. elegans* is less stressful than conventional manipulation techniques, as the worms are manipulated in an environment which is very similar to their natural environment, microfluidics keeps the worms in a less stressed state, which is important for accurate neuronal behavior studies. The use of polydimethylsiloxane (PDMS) for the fabrication of these microfluidic devices has additional advantages in this regard because of its permeability to gases, allowing essential oxygen to diffuse into the microfluidic channels. Furthermore, PDMS provides rapid and cost-effective prototyping [4], which is very useful for academic research labs to quickly test their ideas or make microdevices of modest cost.

The controlled transport of *C. elegans* in high-throughput microfluidic devices requires controlled movement of fluids in a significant number of microchannels, which consequently necessitates microvalve arrays. While a variety of microfluidic valves exist, those made of PDMS that are pneumatically actuated have demonstrated the best ability to be arranged into large arrays [5]. These microvalves, called Quake microvalves, are commonly used in PDMS-based microfluidic devices for *C. elegans* because of their ease of operation. However, Quake microvalves require a rounded channel profile, which necessitates cleanroom facilities for molds or complicated fabrication processes [6].

A cheaper and simpler alternative to Quake valves are doormat-style microvalves [6], whose functionality is independent of channel cross-section, so soft lithography molds for them can be made outside the cleanroom by knife cutting of adhesive vinyl films [7] or other techniques. Hence, these microvalves are ideal for rapid and cost-effective prototyping. Unfortunately, doormat-style microvalves are difficult to produce in high numbers or densities (unlike Quake microvalves) as microvalve arrays, as doormat-style microvalves have a valve-seat in their design (Quake microvalves do not) that requires additional manufacturing steps and considerations. First, the valve seat must be masked during the valve membrane bonding step to prevent permanent attachment of the membrane to the valve seat. Performing this masking on large numbers and on small valve seats can be difficult. Second, alignment between the valve seat and the valve chamber is critical for the valves to function and is more challenging than the alignment of Quake valves. Furthermore, alignment can be difficult at the microscale with flexible substrates like PDMS. Altogether, these issues make doormat-

style microvalves difficult to produce in high densities when compared to Quake microvalves. Nevertheless, as doormat style valves have significant advantages for rapid prototyping, methods to overcome these limitations would be of significant value. This chapter will present methods to overcome these limitations.

There are basically three components of a doormat-style microvalve: the valve chamber, a flexible PDMS actuating membrane, and the valve seat. During fabrication, each of these components is realized in three separate PDMS subcomponents/layers (to be called flow-layer, actuating membrane, and valve-layer respectively in this presentation) that are aligned to each other and then bonded together to fabricate the valves. The flow-layer encompasses all microchannels in which the fluid sample of interest would flow or be manipulated and hence contains the valve-seats, while the valve-layer encompasses all valve chambers and the microchannels that are used to pneumatically pressurize those valve chambers. The actuating membrane sits between and separates these two layers.

Doormat-style microvalves have recently been fabricated in high density in an all-PDMS substrate [8]. The fabrication procedure utilizes corona bonding to bond the valve-layer to the flow-layer, which can work well, but efficient repeatable alignment in corona bonding requires trained hands or alignment hardware, as good quality corona-induced irreversible bonding is instantaneous with little opportunity to correct misaligned layers. A method for correcting misaligned layers could be very beneficial in the prototyping process of PDMS-based microfluidic devices. Additionally, Mosadegh et al. used precisely aligned stamping of PDMS residual oligomers to selectively block bonding of the valve-seats. Furthermore, repeatable use of the same

PDMS stamp for many identical prototypes can be problematic, as the stamp quickly loses its ability to deposit sufficient oligomers for effective masking [9].

In this work, a new fabrication protocol is presented that enables microfluidic researchers to readily build complex microfluidic circuits that require hundreds of pneumatic doormat-style microvalves in PDMS substrates with relative ease and for low cost. The simple protocol aids rapid prototyping, bypasses some drawbacks of corona bonding, does not require cleanroom use, and can be used for high or low-aspect ratio microchannels of any channel cross-section profile. This work also reports for the first time the use of a CO_2 laser in building micromolds using laser cutting of adhesive vinyl tapes.

The key innovative feature of the manufacturing protocol is exploitation of the tendency of partially cured, actuating PDMS membranes (~16.4µm thick) to reversibly bond to a valve ceiling and avoid being irreversibly bonded to the valve-seat during the final assembly process (a major drawback of doormat-style microvalves [6]). Since partially-cured bonding is utilized (which is not instantaneous and has good bonding quality as compared to corona bonding [10]) for bonding the flow-layer to the valve-layer, a good manual alignment can easily be achieved as an alignment error can be corrected by safely separating the misaligned layers before re-aligning. Design optimization and fabrication characterization has been completed showing high valve yield and the applicability of the technique to custom microfluidic projects.

An application of this new microvalve array manufacturing technique is demonstrated by fabricating a microfluidic interface for 32 wells of a 96 well plate, which is then used to automate high throughput genetic screening of *C.elegans*. The

well plate interface is designed to provide specific access to the contents of any of the 32 wells at any given time and deliver the contents of that well to a single output well. That output-well could be connected to a microfluidic sorting / imaging or a behavioral analysis device for high-throughput neuronal-behavior analysis of worms with known genetic-makeup [2], [11].

Materials and Methods

Mold Fabrication

All soft lithography molds were made by cutting the mold pattern in adhesive vinyl tape (Gerber Instachange Removable Film, Gerber Scientific Products, Tolland, CT, USA) by laser cutting and then placing the pattern in a polystyrene Petri dish to make the final mold. A CO_2 laser (VLS 3.60, Universal Laser Systems, AZ, USA) was calibrated to provide the right settings to cut the tape and do minimum damage to the tape's carrier. Leaving the tape's carrier with minimum damage facilitated easy manipulation of the cut-out pattern as the carrier provides the structural strength to hold the cut-tape pieces relative to each other. The mold fabrication process is depicted in Fig. 3.1.

Fig. 3.1(a) shows the tape (which will form the PDMS mold) attached to its carrier. This tape is placed on the laser cutting surface and the laser probe is focused according to the total thickness of the tape and carrier. Using an appropriate laser power, cutting speed, and resolution, the cutting is performed as shown in Fig. 3.1(b). Once the first section of tape is cut, a second piece of tape is separated from its carrier and placed on the cut tape and rolled flat as shown in Fig. 3.1(c) and (d), respectively.

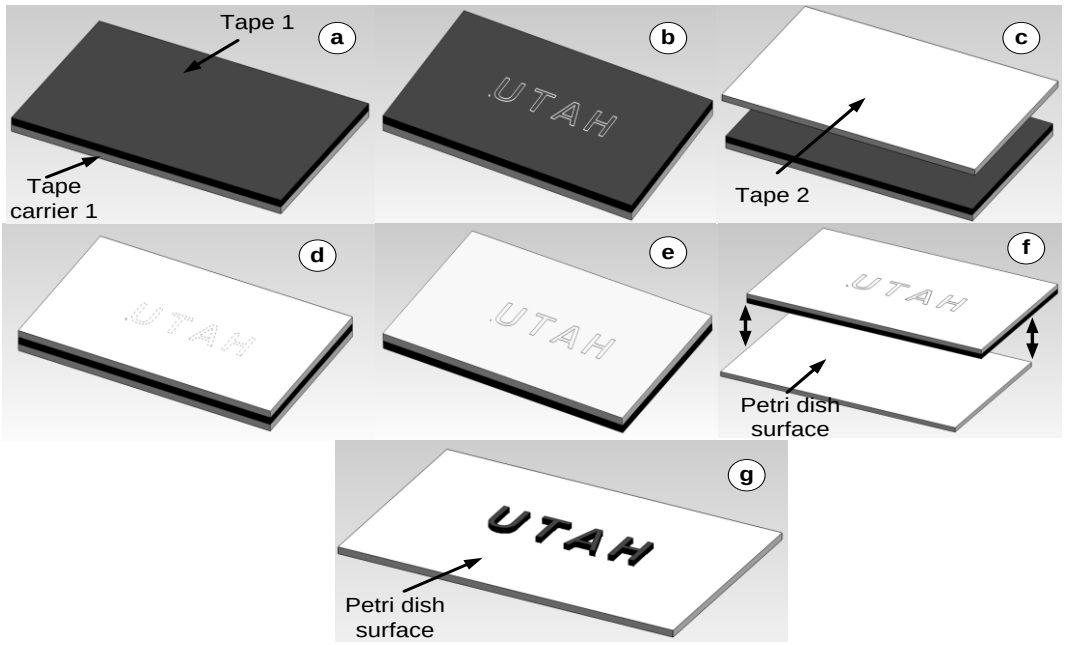

Figure 3.1. A fabrication schematic for making a PDMS mold using laser cutting. (a) A piece of adhesive vinyl tape (Tape-1), carrier attached; (b) the tape undergoes laser cutting of the word "Utah"; (c) another piece of tape (with its carrier removed) is placed on Tape-1 with the cut pattern; (d) Tape-2 rolled flat over Tape-1, along with Tape-1's carrier; (e) Tape-1's carrier is gently removed and the cut and uncut parts in Tape-1 remain attached to Tape-2; (f) the Tape-1 and Tape-2 combination is rolled flat on a Petri dish surface; (g) The two layers of tape are gently peeled off either altogether or one-by-one. The cut-out pattern remains adhesively bonded to the Petri dish surface while the uncut pattern remains attached to Tape-2.

The rolling should be done gradually from one end to other end of the tape to ensure there is a minimum amount of trapped air bubbles between two consecutive layers of tape. Afterwards the tape laminate shown in Fig. 3.1(d) is turned upside down and the bottom carrier (Tape-1's carrier) is removed (Fig. 3.1e). Care is taken not to peel off the cut structures in Tape-1. The tape laminate shown in Fig. 3.1(e) is then rolled flat on a 150 x 15 mm polystyrene Petri dish (Part #. 351058, Becton Dickson Labware, Franklin Lakes, NJ, USA) from one end to the other (Fig. 3.1f). Again, care is taken to prevent bubbles between the Petri dish surface and the tape laminate. These trapped air bubbles

can be seen through the Petri dish and easily eliminated by repressing the tape against the mold.

In the end, Tape-2 and uncut portions of Tape-1 are peeled-off using tweezers, leaving the patterned Tape-1 features on the Petri dish surface as shown in Fig. 3.1(g). The patterned Tape-1 features are further gently rolled to ensure adhesion to the Petri dish surface.

PDMS Microvalve Array Fabrication

The PDMS doormat-style microvalve array is built in three parts or layers that are later bonded together with appropriate alignment. These three parts are the: flow-layer, valve-layer, and the actuating membrane. All the PDMS (Slygard® 184 Silicone Elastomer, Dow Corning, MI, USA) used in this work had a base-to-curing ratio of 10:1.

Molding and surface treatment of the valve-layer. Fig. 3.2 shows the fabrication protocol for the valve-layer. In part (a) the mold is made by laser cutting of adhesive vinyl tape, as described in Fig. 3.1. The thickness of a single layer of the vinyl tape used in this work is ~110 µm. In Fig. 3.2(b), PDMS is poured in the mold with a depth of ~2.2 mm and cured in an oven at 62˚C for at least 5 hours. Later the part is peeled-off from the mold as depicted in Fig. 3.2(c).

Since these are pneumatic membrane microvalves, access holes for pneumatic pressurization of the valve chambers are cored in the molded part using a coring tool (Harris Uni-core 15075, Ted Pella Inc., CA, USA) as shown in Fig. 3.2(d).

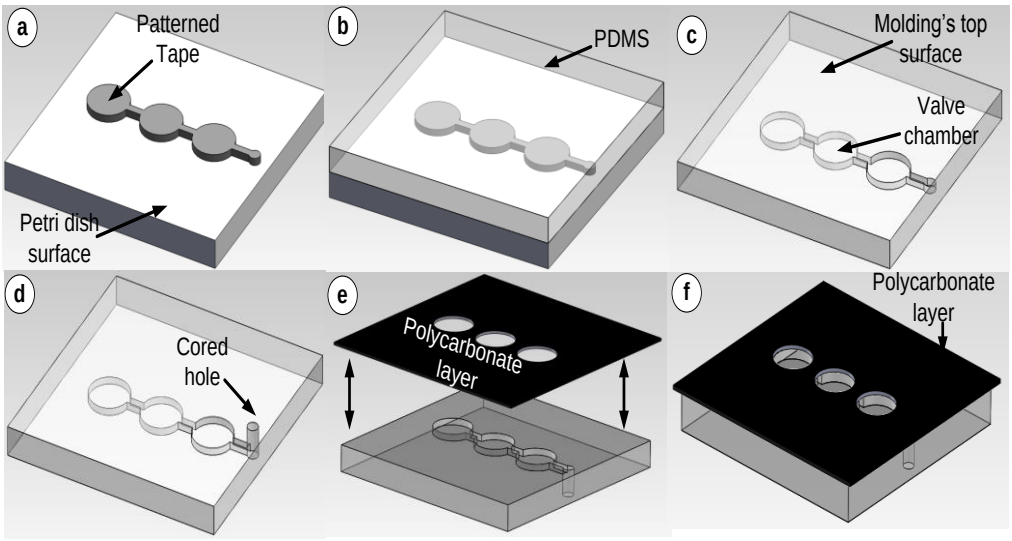

Figure 3.2. Fabrication schematic of valve-layer. (a) valve-layer mold; (b) PDMS is poured in the mold and cured; (c) the PDMS molded part is removed from the mold; (d) An access hole is cored for pneumatic pressurization of the valves; (e) & (f) A patterned polycarbonate layer is temporarily attached to the valve-layer's bottom face.

At this point, the valve-layer is turned upside-down, and a ~0.12-mm thick patterned polycarbonate (Lexan FR83-CLEAR, SABIC Polymershapes, CA, USA) masking layer is placed on top of it. The masking polycarbonate layer is patterned (selectively cut) by the laser in such a way so as to cover all parts of the inverted valve-layer except the valve ceilings as shown in Fig. 3.2 parts (e) and (f). The polycarbonate layer has two sides: a smooth side and a rough side. The smooth side reversibly bonds better to the PDMS surface than the rough side. Hence, the polycarbonate layer is patterned in such a way that the smooth side interfaces with the PDMS surface. The placement of the polycarbonate layer is done manually without any alignment hardware. At the stage shown in Fig. 3.2 (f), the valve-layer is placed in a vacuum chamber at -88 kPa for 75 minutes for vacuum deposition of triethoxy-silane (SIT8175.0-50GM, Gelest Inc., Morrisville, PA, USA) on the exposed valve ceiling.

Triethoxy-silane is used to enable reversible bonding of the actuating membrane to the valve ceiling. After vacuum deposition of the triethoxy-silane, the polycarbonate masking layer is removed from the valve-layer.

Preparation and attachment of the actuating membrane. A partially cured PDMS membrane to serve as the actuating membrane is prepared by spin coating PDMS on a poly(methyl methacrylate) (PMMA) wafer at 2800 rpm at a ramp of 340 rpm/s and then baked in an oven at 62 ˚C for 40 minutes. The valve-layer and the partially cured membrane are activated for corona bonding by using a corona discharge machine (LM4243-05, Enercon Industries Corporation, WI) and contacted as shown in Fig. 3.3 after step 1. Both contacted pieces are placed in an oven at 62 ˚C for 30 minutes to increase the strength of bonding and also to deactivate the valve-layer for any further corona bonding. After taking the bonded pieces out of the oven, they are allowed to cool for 5 minutes at room temperature. The valve-layer is then gently pulled up against the PMMA wafer as depicted in step 2 of Fig. 3.3. This detaches the partially cured membrane (now permanently bonded to the valve-layer) from the PMMA wafer. Afterwards the partially cured membrane is gently pushed up against the valve chamber by pressure from an air gun as shown in step 3 of Fig. 3.3. The membrane, as it is partially cured, will have a tendency to reversibly bond to the valve ceiling due to the significant presence of uncrosslinked oligomers [12]. This adhesion creates a contact area between the valve ceiling and membrane, which is referred to as valve-membrane overlap. Fig. 3.4 parts (g) and (h) illustrate the bonded, partially cured membrane and the valve-membrane overlap in the valve-layer, respectively.

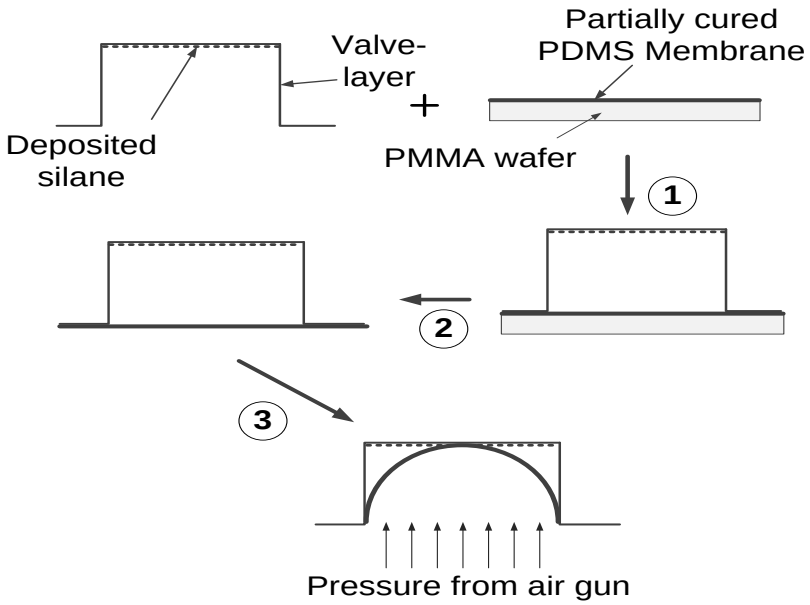

Figure 3.3. Three steps of bonding partially cured PDMS membrane to the valve-layer and creating valve-membrane overlap.

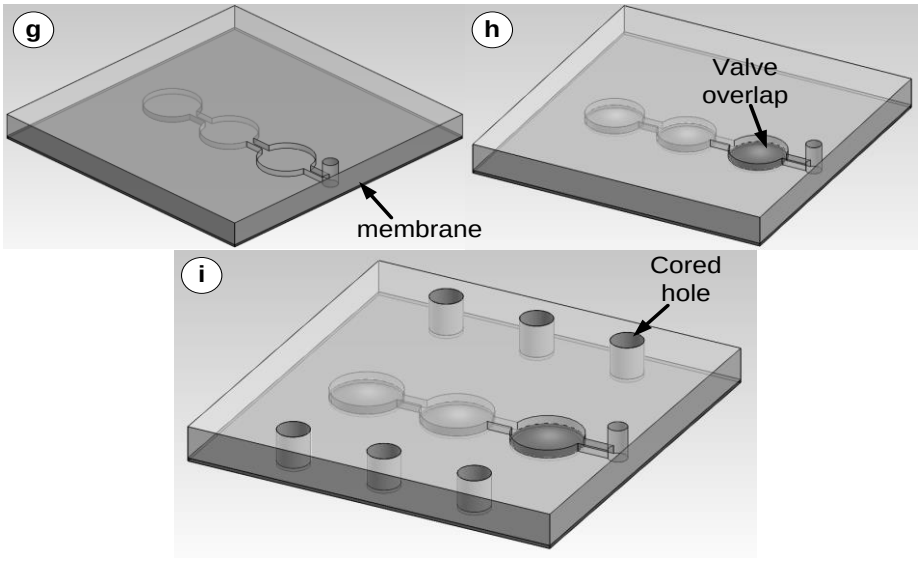

Figure 3.4. Fabrication schematic of the valve-layer where each fabrication stage is denoted by a small letter. (g) A partially cured membrane is bonded to the bottom of the valve-layer; (h) Membrane is made to temporarily adhere to the valve ceiling by an air gun to create Valve-membrane overlap; (i) Access holes are cored for inlets and outlets for microchannels in the flow-layer.

In the end, through-holes are cored with a coring tool (Harris Uni-core 15075, Ted Pella Inc., CA, USA) in the valve-layer for inlets and outlets for the microfluidic circuit in the flow-layer as illustrated in part (i) of Fig. 3.4.

Molding of the flow-layer. Fig. 3.5 shows the fabrication protocol for the flow-layer. In part (a) the mold is made by laser cutting of the adhesive vinyl tape, as described in Fig. 3.1. In part (b), PDMS is poured in the mold with a depth of ~2.2 mm and cured in an oven at 62 ˚C for 1 hour, leaving the molded part partially cured. Later the molded part is peeled off from the mold as depicted in part (c), which now becomes the valve-layer.

Bonding of the valve-layer to the flow-layer. Fig. 3.6(a) shows the bonding arrangement of the valve-layer and the flow-layer for the final realization of the microvalve array. To enable simple alignment, both layers are kept reversibly bonded to PMMA plates, which simplifies handling and reduces misalignment errors associated with the flexibility of PDMS. As both interfacing surfaces are partially cured, once appropriate alignment is achieved, the layers are placed in contact, and trapped air bubbles are squeezed out using gentle, moving pressure. Trapped bubbles close to the valve ceilings are squeezed out by pinching using the edges of tweezers as pinching by fingers or similar objects could depress the valve ceiling and irreversibly bond the overlapped partially cured membrane to the valve-seat on the flow-layer, which will render the valve nonfunctional. After the layers have been aligned, contacted, and the bubbles removed, the whole assembly is placed in the oven at 62 ˚C for at least 5 hours. Fig. 3.6(b) shows the fully fabricated microvalve array.

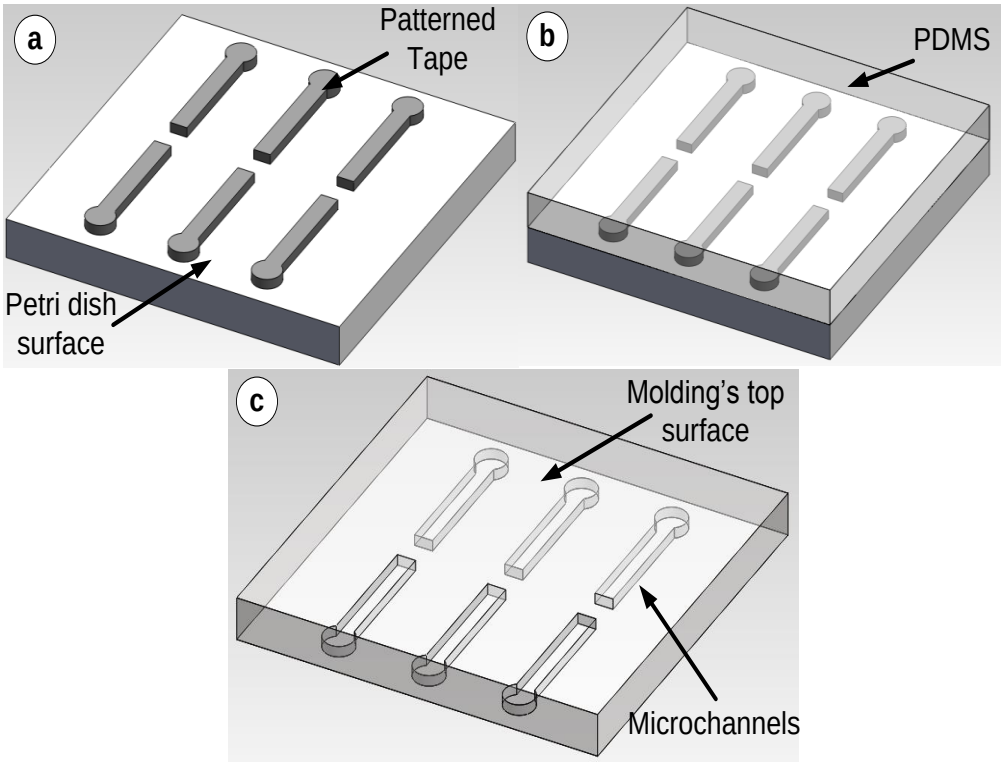

Figure 3.5. Fabrication schematic of the flow-layer. (a) Microstructures are laser cut and placed on the Petri dish surface; (b) PDMS is poured on the Petri dish surface and partially cured; (c) The partially-cured flow layer is peeled off.

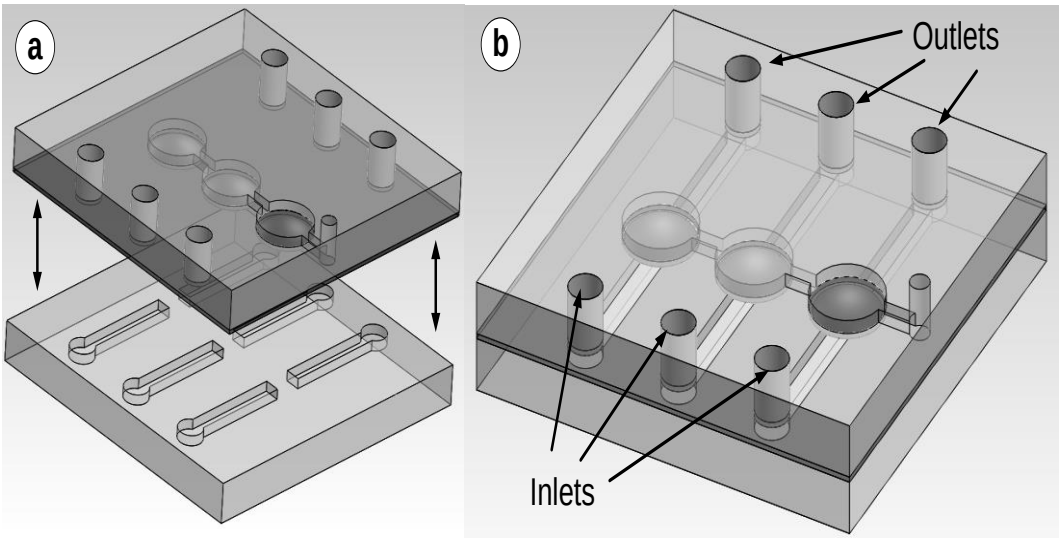

Figure 3.6. (a) Depiction of bonding arrangement of the valve-layer and the flow-layer; (b) Fully-fabricated microvalve array.

Design Optimization

In order to determine the parameters that optimize manufacturing and function of the presented microvalve arrays, experiments and computer simulations were carried out. Key design parameters that affect this valve-membrane overlap need to be determined so that the technique can be practically used by the microfluidics research community.

The basic principle that underlies this new microvalve array fabrication technique is the ability of the actuating membrane to avoid being bonded to the valve-seat in flow-layer during manufacturing, which requires temporary membrane adhesion to the valve ceiling. The ability to increase this valve-membrane contact area is related to the flexibility of the membrane, which can be physically quantified using the stiffness of the membrane. Membrane stiffness depends on membrane shape, boundary conditions and membrane material [13]. As boundary conditions and material are practically difficult to vary in this case, changing the membrane's shape by changing the valve-chamber's shape is more feasible. Hence, experiments and simulations were focused on discovering valve-chamber shapes and sizes to give the highest yield of microvalves or promote valve-membrane contact area. We experimented on three valve-chamber shapes: circle, square, and capsule (Fig. 3.7).

Experiments. Microvalve arrays with valve chambers of different sizes and shapes were made using the protocols described in sections 2.1 and 2.2. The relative amount of valve-membrane overlap is quantified by a contact ratio which is defined by

$$contact\ ratio = \frac{A_1}{A_2}$$

where A_1 (contact area) and A_2 (area of valve chamber) are defined in Fig. 3.8. ImageJ

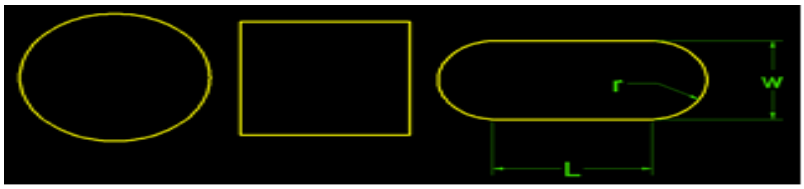

Figure 3.7. Different valve-chamber shapes tested to determine key design parameters for encouraging valve-membrane overlap. For capsule: L ~ 1.35w, r = w/2.

software (National Institute of Health, Bethesda, MD, USA) was used to measure areas A1 and A2 (depicted in Fig. 3.8) from images of different fabricated valve shapes and sizes collected with a microscope.

Simulations. Membranes of different shapes and sizes were simulated in COMSOL multiphysics software (COMSOL, Inc., Los Angeles, CA, USA) using the solid mechanics module.

PDMS was assumed to be a linear elastic material, which is a reasonable approximation based on experiments described in the literature [14]. The PDMS properties were estimated from literature data as follows:

1. Poisson's ratio = 0.47 [15]; [16]
2. Young's Modulus = 1.6 x 10^6 Pa [17]
3. Density = 920 kg/m^3 [18]

These values account for the base-to-curing agent ratio, curing time, and temperature of the partially cured membrane used in this work. The thickness of the PDMS membrane used in the physical devices was measured for each experiment by a Profilometer (Profilometer Tencor P-10, KLA-Tencor Milpitas, CA) and amounted to 16.4 ± 0.9 µm. This PDMS membrane thickness was used in all simulations.

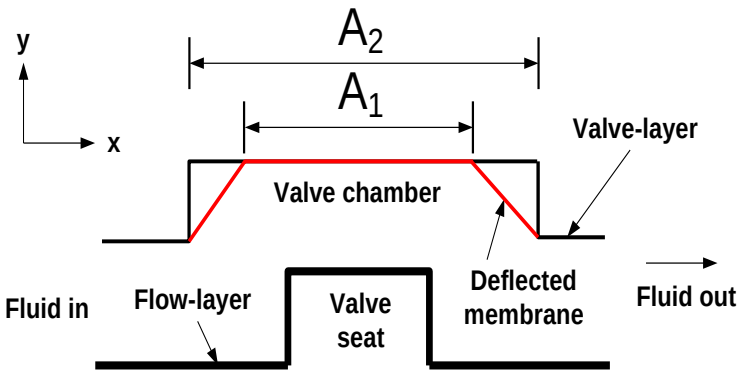

Figure 3.8. Depiction of areas A_1 and A_2 and the valve-membrane contact area. The higher the contact ratio, the greater the tolerance of misalignment between valve-layer (represented by thinner line) and flow-layer (represented by a thicker line). Larger contact areas help prevent the valve-seat from being irreversibly bonded to the actuating membrane, which helps keep the valve functional.

The membrane is assumed to be linear elastic with a stress-strain relationship defined by Duhamel-Hooke's law:

$$s = s_0 + C : (\varepsilon - \varepsilon_0 - \alpha\theta)$$

where s_0 is the initial stress, ε_0 is the initial strain, C is the elasticity tensor, θ is the change in temperature, and α is the thermal expansion coefficient.

The membranes were loaded with a total force of 1 μN distributed across the surface of the membrane, i.e., in the y-direction according to Fig. 3.8.

Membrane stiffness at different membrane sizes and shapes was computed from simulations. The resulting stiffness values were plotted against respective valve-chamber areas using MagicPlot 2.3 (Magicplot Systems, LLC, St. Petersburg, Russia). Furthermore, the plot of stiffness versus valve-chamber area was numerically differentiated in MagicPlot 2.3 to obtain the rate of change of membrane stiffness with change in valve-chamber area.

Test Methods

To test the function of the fabricated valves, de-ionized water was mixed with food color dyes and flowed through the microvalve array circuits to check for any valve leaks or failure.

To test the operation of the valves with *C.elegans*, ~50 wild-type *C.elegans* were flowed through the 32-well microfluidic manifold to check the flow of worms through microvalves and microchannels. These worms were flowed from three of the 32 wells and transported to the main output well. The *C.elegans* had ages ranging from L1 to adults and were suspended in M9 buffer solution.

Results and Analysis

Mold Fabrication

Fig. 3.9 shows molds fabricated by laser cutting of adhesive vinyl tape. One mold was able to produce three molded parts before some of the microstructured parts began to peel off, suggesting that this method is primarily useful for rapid prototyping applications.

Experience showed that the most critical parts of the mold fabrication process were parts (d) to part (e) in Fig. 3.1, where the carrier of the patterned tape (Tape-1) was removed. Even though the carrier was loosely adhered to the patterned tape, during the carrier's separation, small and narrow microstructures (~100 μm) tended to be pulled off by the carrier. This phenomena discouraged complex mold designs. However, this problem was avoided by turning the tape laminate at stage (d) (Fig. 3.1) upside down and by gradually peeling-off the carrier and holding down the rest of the laminate.

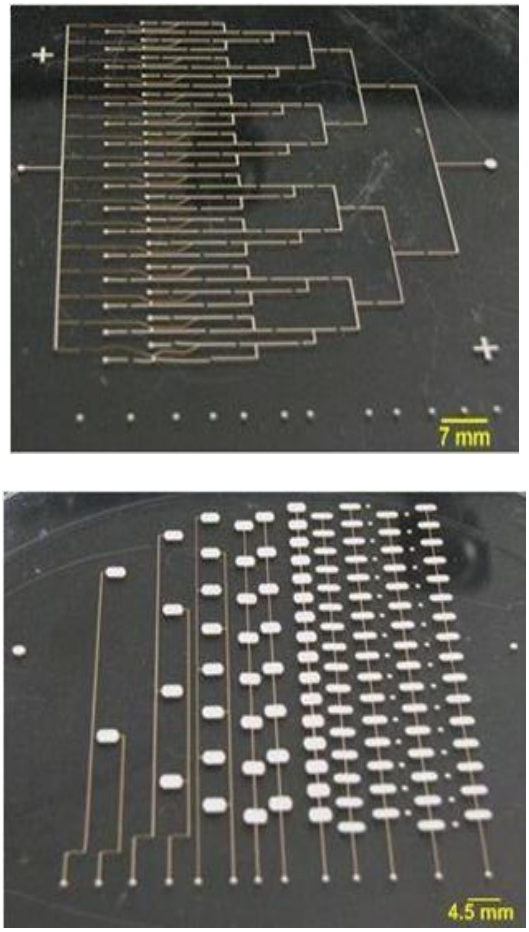

Figure 3.9. Molds fabricated by laser cutting of adhesive vinyl tapes on polystyrene Petri dishes. Top: Flow-layer mold. Bottom: Valve-layer mold

Using this process one can easily observe any microstructure being mistakenly peeled off by tape's carrier and consequently reapply compression at that point by tweezers to reattach a peeled off microstructure to the Tape-2 transfer layer. It was also observed that keeping the peeling angle θ (the obtuse angle the Tape-1 carrier makes with the Tape-1/Tape-2 laminate during Tape-1 carrier separation from the laminate, from part d to part e in Fig. 3.1) as large as possible helped prevent thinner microstructures in Tape-1 from being mistakenly peeled off.

Valve-membrane Overlap

As noted previously, the valve-membrane overlap is critical in the fabrication process for these doormat-style valves. Fig. 3.10 shows the simulated displacement of the membranes in the different valve designs. Fig. 3.11 shows images under a microscope of the different valve designs with the membrane under pressure and adhered to the valve ceiling. In comparing Fig. 3.10 and Fig. 3.11, it is clear that the displacement contours determined in these simulations match the contours of the respective valve-membrane overlap in the microscope images.

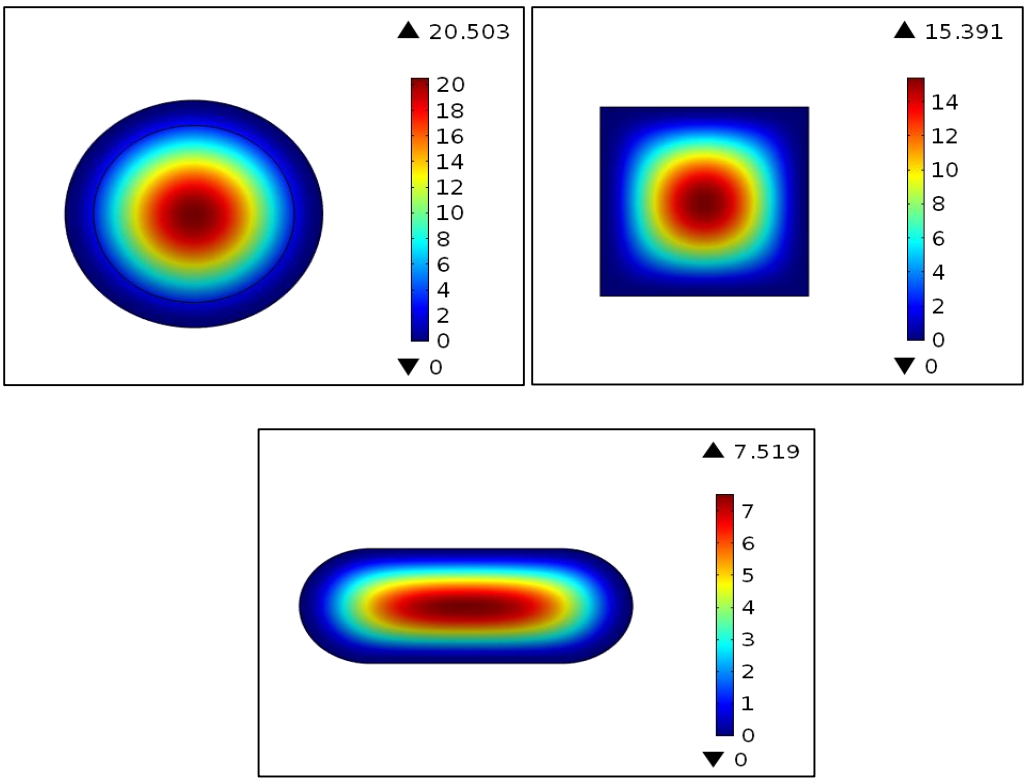

Figure 3.10. The interfacing membrane surface is the surface that interfaces with the valve-seat when the membrane is actuated. The figures show surface displacement (μm), normal to the interfacing surface of the membrane for all three shapes, as computed by COMSOL simulations. The membranes were displaced by a force of 1 μN acting normal to the interfacing surface of the membrane.

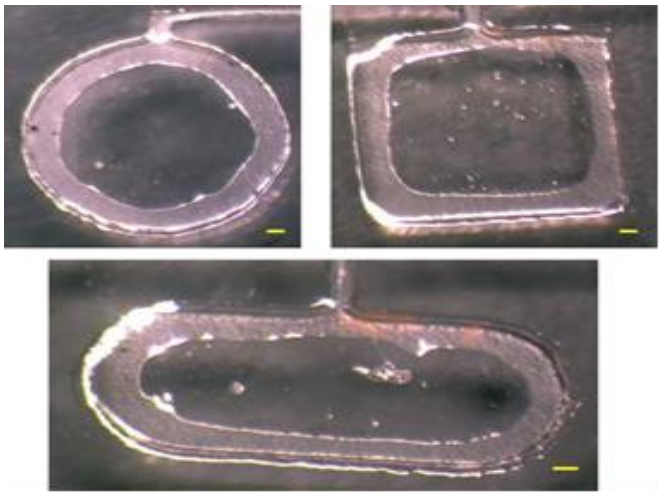

Figure 3.11. The valve-membrane overlaps of three valve shapes (circle, square, and capsule) are visible as dark gray inner regions, while the unbounded area appears lighter (scale bar: 220 μm).

This comparison of Fig. 3.10 and Fig. 3.11 suggests that the simulation results are useful for analyzing the operation and function of the different valve designs and potentially predicting which shapes will provide the best valve-membrane overlap for fabrication purposes. Physically, the stable valve-membrane overlap occurs when an equilibrium state is achieved between two forces: the membrane spring force and intermolecular surface forces.

The stiffer the membrane (the higher the spring constant), the more difficult it is for the intermolecular adhesive forces to keep the membrane reversibly bound to the valve ceiling. For the purposes of this work, the membrane stiffness and the resulting spring forces depend primarily on the thickness of the membrane and the area and shape of the membrane. The elastic modulus of the material and ceiling height are constant in this work and so are less important for the design. Larger membrane areas decrease the overall stiffness of the membrane and result in a concomitant increase in valve-chamber

area, which is directly related to the intermolecular surface forces. Consequently valve-membrane overlap increases, thereby increasing the contact ratio.

The behavior is depicted in Fig. 3.12. The higher the value of the contact ratio the more margin is available for alignment error between the valve-layer and the flow-layer, leading to higher manufacturing yields. This improved yield leads to more flexibility in rapid prototyping of PDMS-based microvalve arrays.

Comparison of Fabricated Valves

Fig. 3.12 shows how the contact ratios of different shapes vary with an increase in valve-chamber area. Circles clearly generate the highest contact ratio, which was expected as they have the lowest stiffness (Fig. 3.13 top).

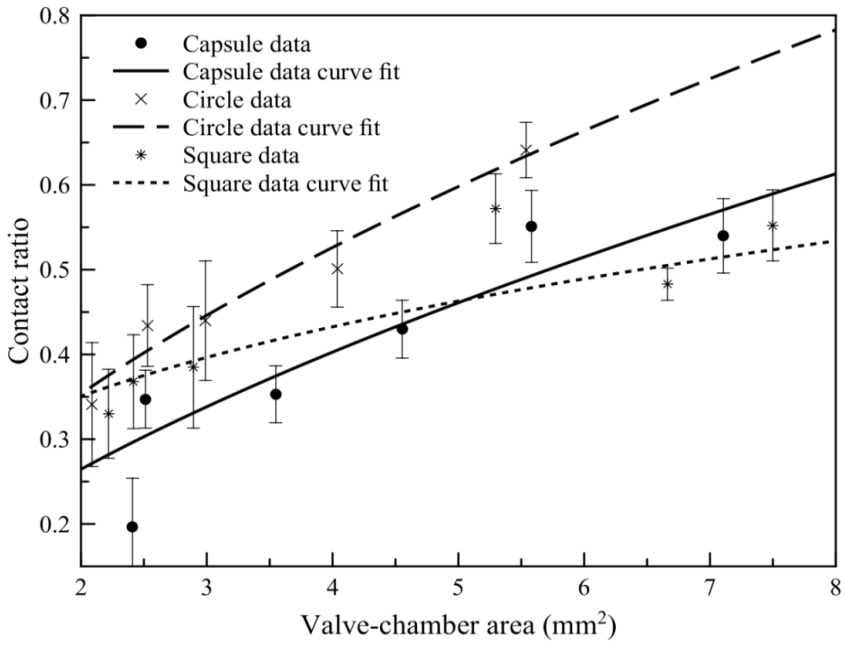

Figure 3.12. Plot of measured contact ratios of valve chambers of three different shapes at various sizes along with their respective curve fits

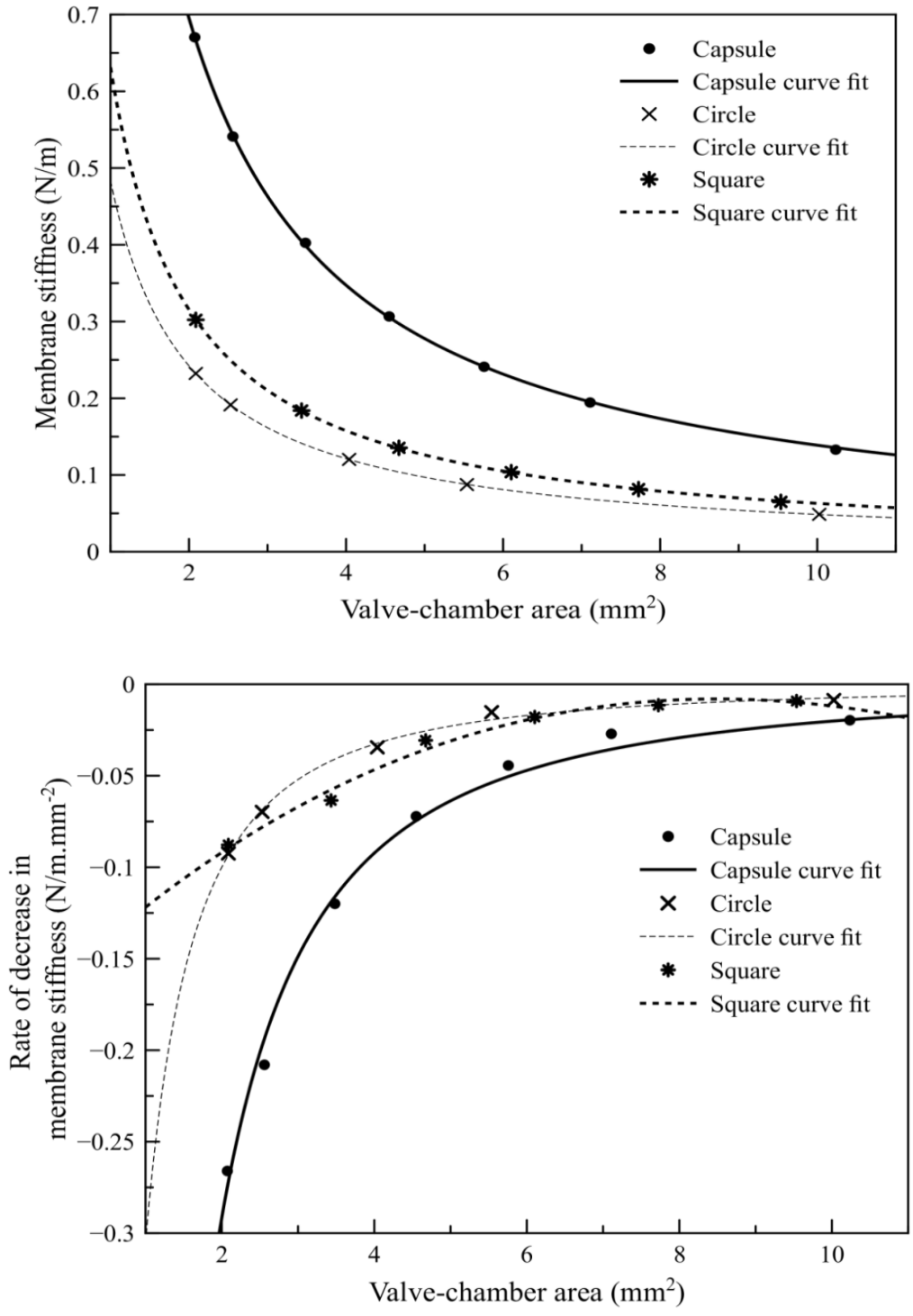

Figure 3.13. Simulation results from COMSOL. Top: Membrane stiffness vs. valve-chamber area of valves of three different shapes and various sizes. Bottom: Rate of decrease of membrane stiffness with an increase in valve-chamber area for three different shapes

However, even though squares have a lower stiffness than the capsules (Fig. 3.13 top), in Fig. 3.13 (bottom) the rate of decrease in stiffness of squares is lower than for the capsules or circles, which explains the similar curve-fit gradients for the circles and capsules and the comparatively lower curve-fit gradient for the squares in Fig. 3.12.

The occurrence of valve-membrane overlap is dependent on the shape of the valve-chamber area. For capsules below 2.5 mm^2 in chamber area, valve-membrane overlap is not observed and if it is observed, the occurrence of valve-membrane overlap is inconsistent. As determined from Fig. 3.13 (top) for a capsule chamber area of 2.5 mm^2, the membrane stiffness is 0.556 N/m. As the valve-membrane overlap is a balance between membrane spring forces and the intermolecular adhesive forces, the membrane stiffness of 0.556 N/m could be the limiting stiffness for all valve-chamber shapes. Beyond this limiting stiffness, the intermolecular adhesive forces would not be able to maintain any valve-membrane overlap. From the curve fits in Fig. 3.13 (top), the limiting valve-chamber areas for squares and circles are at the membrane stiffness of 0.556 N/m are 1.1 mm^2 and 0.9 mm^2, respectively. These computed limiting valve-chamber areas generally agree with the experimentally observed values as shown in Table 3.1.

As a general consideration, the fabrication protocol presented is designed to help researchers with rapid prototyping and testing of microfluidic chip design ideas where alignment hardware may not be readily available or its use desired. Fabricating valve-chamber areas less than or equal to the limiting chamber areas necessitates accurate alignment between valve-layer and flow-layer, which would likely require alignment hardware, possibly eliminating some of the value of the presented fabrication method.

Table 3.1. Delimiting valve-chamber areas of circle and square shapes

	Capsule	**Square**	**Circle**
Max. valve-chamber area observed **without** valve-membrane overlap (mm^2)	1.4	0.9	1.0
Limiting valve-chamber area from curve-fit equations (mm^2)	N/A	1.1	0.9

The membrane yield also appeared to be a function of shape. During step 2 of Fig. 3.3 the partially cured membrane experiences significant adhesive forces from the PMMA surface. These forces can cause membranes to tear, which results in valve failure. This failure was frequently observed in circle and square shape chambers at large sizes (> 4 mm^2 for circle and > 5.5 mm^2 for square). From Fig. 3.13 (top) the average membrane stiffness at these sizes is ~0.118 N/m. This value is never attained by capsules at the sizes tested. Thus, the capsule shape is recommended for sizes larger than 4 mm^2 for circle and 5.5 mm^2 for square. And for lower sizes (up to 2.5 mm^2) almost all shapes can be used; however, the capsule shape provides a benefit of being shorter in one direction.

32-Wellplate Interface Test Results

The fabricated valve arrays were tested to determine their ability to collect and distribute *C. elegans* to appropriate wells in a 96 well plate. For these tests a microfluidic 32-well manifold was fabricated. The microvalves in the microfluidic 32-

well manifold (shown in Fig. 3.14) were pneumatically pressurized at 4 psi. Pressures higher than 5 psi usually resulted in valve failure, but the valves operated well below this level. Some microvalves ended up nonfunctional due to unintentional irreversible bonding of the membrane to valve-seat. In high-throughput microfluidic systems that uses a number of microvalves, such nonfunctional valves can be very detrimental to the functionality of the system. Since a single nonfunctional microvalve can block access to more than one microchannel, depending on the location of the microvalve in the microfluidic circuit, designing critically located microvalves with a reliable valve-chamber area (i.e., a larger valve-chamber area) to get a large valve-membrane overlap is suggested.

When the microvalves were initially pressurized for the first test, the actuating membranes did not instantly separate from the valve ceiling (due to the valve-membrane overlap). However, maintaining the pressure for 5 minutes or less eventually separated the actuating membrane from the valve ceiling. After this initial separation, the doormat-style valve could be turned ON/OFF instantly.

Out of 110 microvalves fabricated in this array (Fig. 3.14), only two proved nonfunctional. *C. elegans* of all sizes found no difficulty in moving through the series of six microvalves that defined a path to a well location, and no worms were lost during transportation from the storage wells to the main output well. Thus, the valve design appeared to work well with *C.elegans* of all sizes.

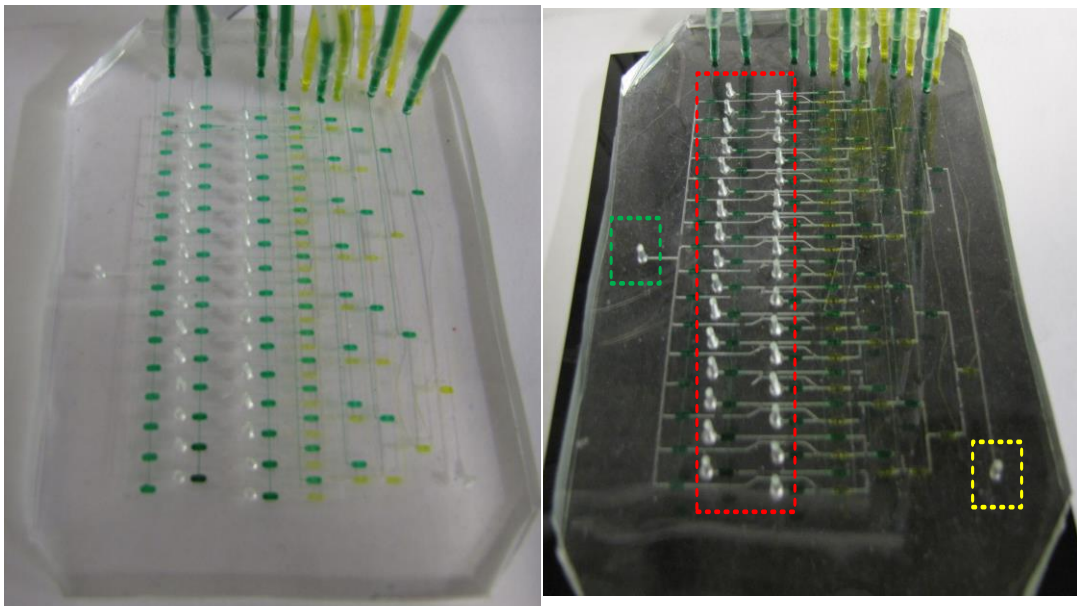

Figure 3.14. The complete microfluidic circuit for a 32-well microfluidic manifold for manipulation of *C. elegans*. Top: 110 capsule-shaped microvalves filled with DI water and food color dyes displaying the circuit for the valve-layer. Bottom: Microchannels in the flow-layer made more visible with a black background. Red-dotted rectangle highlights inputs from 32-wells called well-inputs. Yellow-dotted rectangle highlights the main output well. Green-dotted rectangle highlights the input for a flush line to clean specific portions of the circuit from debris. With orientation of the microfluidic manifold as shown in the figure, the horizontal spacing between well-inputs is 10 mm, and the vertical spacing is 4.5 mm.

Manufacturing Options

During fabrication of the microvalve arrays and following testing, it was determined that some of the manufacturing protocols could be modified by the user for their specific needs. Therefore, it is possible to eliminate steps that involve silane deposition and placement of the polycarbonate masking layer in the valve-layer fabrication. This can be done by further curing the valve-layer mold obtained in Fig. 3.2(c) at 115 ˚C for 2 hours, ensuring all uncrosslinked oligomers have been eliminated.

A second observation was that the adhesive vinyl tape has an inherent surface roughness that serves to hinder the partially cured PDMS membranes from irreversibly bonding to the valve ceiling. Hence, the fabrication protocols described in this presentation may not work properly with valve-layer molds made from very smooth tapes or photolithographically generated molds where the surface finish of the molds is very smooth.

A third observation was that it is also possible to utilize corona-bonding instead of partially cured bonding for the irreversible bond between the valve-layer and the flow-layer. In this case the fabrication protocol would be similar as described earlier with all partially cured parts being fully-cured. There would not be any need of silane deposition and polycarbonate masking layer. However, once the valve-layer has been bonded to the actuating membrane, it would be important to place these bonded parts in the oven at 62 ˚C for at least 30 minutes. This ensures that all corona activated surfaces have become inactive so that when valve-membrane overlap occurs the membrane does not irreversibly bond to the valve ceiling. On the other hand, this fabrication protocol limits the minimum size for the valve-chamber area for sufficient valve-membrane overlap as uncrosslinked oligomers are no longer present to encourage adhesion between the actuating membrane and valve ceiling. Consequently, the stiffness of the membrane has to be decreased by increasing the valve-chamber area in order to encourage valve-membrane overlap. Furthermore, since corona bonding is instantaneous, it leaves less room for the correction of an alignment-error during the alignment of the valve-layer to the flow-layer. However, it is a faster alternative to the protocol presented in this work.

Conclusions

We have introduced a new fabrication protocol for prototyping doormat-style microvalve arrays in PDMS substrates. The protocol is simple and cost-effectively utilizes the rapid prototyping capabilities of soft lithography and laser cutting of adhesive vinyl film for making micromolds. It has been shown in the protocol that by manipulating the stiffness of the actuating membrane by varying the valve-chamber area/shape, doormat-style microvalves can be easily fabricated in arrays. Three commonly used valve-chamber shapes (circle, square and capsule) have been investigated where simulated results agree with experimental observations. These observations highlight design parameters and configurations that can influence the yield of these valves. A unique application of these microvalves has been demonstrated by building a microfluidic 32-well plate interface for high-throughput manipulation of *C. elegans*. Using this new protocol, researchers can quickly test their ideas by building custom low-cost microfluidic devices for biomedical studies on *C. elegans* or other applications.

References

[1] Lynch, Z., 2004, "Neurotechnology and Society (2010-2060)," Ann. N. Y. Acad. Sci., **1013**, pp. 229–233, doi: 10.1196/annals.1305.016

[2] Ben-Yakar, A., Chronis, N., and Lu, H., 2009, "Microfluidics for the Analysis of Behavior, Nerve Regeneration, and Neural Cell Biology in C. elegans," Curr. Opin. Neurobiol., **19**(5), pp. 561–567, doi: 10.1016/j.conb.2009.10.010

[3] Lockery, S., 2007, "Channeling the Worm: Microfluidic Devices for Nematode Neurobiology," Nat. Methods, **4**(9), pp. 691–692

[4] McDonald J. C., and Whitesides, G. M., 2002, “Poly(dimethylsiloxane) as a

Material for Fabricating Microfluidic Devices.," Acc. Chem. Res., **35**(7), pp. 491–499, doi: 10.1021/ar010110q

[5] Thorsen, T., Maerkl, S. J., and Quake, S., R., 2002, "Microfluidic Large-scale Integration," Science, **298**(5593), pp. 580–584, doi: 10.1126/science.1076996.

[6] Au, A. K., Lai, H., Utela, B. R., and Folch, A., 2011, "Microvalves and Micropumps for BioMEMS," Micromachines, **2**, pp. 179–220, doi: 10.3390/mi2020179

[7] Bartholomeusz, D., 2005, "Xurography: Rapid Prototyping of Microstructures using a Cutting Plotter," J. Microelectromech. Sys., **14**(6), pp. 1364–1374

[8] Mosadegh, B., Tavana, H., Lesher-Perez, S. C., and Takayama, S., 2011, "High-Density Fabrication of Normally Closed Microfluidic Valves by Patterned Deactivation of Oxidized Polydimethylsiloxane," Lab Chip, **11**(4), pp. 738–742, doi: 10.1039/c01c00112k

[9] Smith, K. A., Gale, B. K., and Conboy, J. C., 2008, "Micropatterned Fluid Lipid Bilayer Arrays Created using a Continuous Flow Microspotter," Anal. Chem., **80**(21), pp. 7980–7987, doi: 10.1021/ac800860u

[10] Eddings, M. A., Johnson, M. A., and Gale, B. K., 2008, "Determining the Optimal PDMS–PDMS Bonding Technique for Microfluidic Devices," J. Micromech. Microeng., **18**(6), doi: 10.1088/0960-1317/18/6/067001

[11] Hulme, S. E., Shevkoplyas, S. S., and Samuel, A., 2008, "Microfluidics: Streamlining Discovery in Worm Biology," Nat. Methods, **5**(7), pp. 589–590

[12] Kroner, E., Maboudian, R., and Arzt, E., 2010, "Adhesion Characteristics of PDMS Surfaces During Repeated Pull-Off Force Measurements," Adv. Eng. Mater., **12**(5), pp. 398–404, doi: 10.1002/adem.201000090

[13] Baumgart, E., 2000, "Stiffness--an Unknown World of Mechanical Science?," Injury, **31**(2), p. S–B14–23

[14] Hohne, D. N., Younger, J. G., and Solomon, M. J., 2009, "Flexible Microfluidic Device for Mechanical Property Characterization of Soft Viscoelastic Solids such as Bacterial Biofilms," Langmuir, **25**(13), pp. 7743–7751, doi: 10.1021/la803413x.

[15] Notbohm, J., Poon, B., and Ravichandran, G., 2012, "Analysis of Nanoindentation of Soft Materials with an Atomic Force Microscope," J. Mater. Res., **27**(01), pp. 229–237, doi: 10.1557/jmr.2011.252

[16] Deuschle, J. K., de Souza, E. J., Arzt, E., and Enders, S., 2010, "Nanoindentation

Studies on Crosslinking and Curing Effects of PDMS," Int. J. Mater. Res., **101**(8), pp. 1014–1023, doi: 10.3139/146.110361

[17] Zhao, Y., and Zhang, X, 2006, "Mechanical Properties Evolution of Polydimethylsiloxane during Crosslinking Process," Mater. Res. Soc. Symp. Proc., pp. 75–81

[18] Armani, D., Liu, C., and Aluru N., 1999, "Re-configurable Fluid Circuits by PDMS Elastomer Micromachining," 12th IEEE Int. Conf. Micro Electro Mech. Syst., pp. 222–227, doi: 10.1109/MEMSYS.1999.746817

CHAPTER 4

MICROFLUIDIC ZEBRAFISH GENOTYPING CHIPS

Abstract

This chapter introduces an innovative method for genotyping 1 to 2 day old zebrafish embryos without sacrificing the life/health of embryos. The method utilizes microfluidic technology to extract/collect a small amount of genetic material (chorionic fluid or fin tissue) from the embryo. Then, using conventional DNA extraction, PCR amplification, and high-resolution melt analysis with fluorescent DNA detection techniques, the embryo is genotyped. This approach was successful and reveals a novel method to genotype zebrafish embryos that can facilitate high-throughput screening while maintaining 100% viability of the embryo.

Introduction

Zebrafish (*Dani rerio*) and zebrafish embryos are extensively used by biologists as a model organism for preclinical drug discovery [1], [2]. The reason for the zebrafish embryos extensive use is that their biological development is sufficiently similar to those of humans [1], the overall drug toxicity in zebrafish embryos is comparable to mammals [1], and there are economic advantages over other mammalian models as

zebrafish embryos have a shorter development time and are cheaper to maintain in research labs [1], [2]. Furthermore, zebrafish embryos are conveniently sized for easy handling, the female fish has high fecundity, and they are optically transparent, which aids in easy visualization of phenotypes [1], [2].

Most current methods and research tools for genotyping zebrafish mutants are tedious and require trained personnel; thus the processes are very slow and expensive. For example for the collection of genetic material for genotyping these fish, mutant embryos have to be either grown into 2-month old adults for fin amputations (manually) or homogenized by grinding in a frozen state, which eliminates the ability to use these fish later [3], [4]. When in search of interesting mutants, these protocols make zebrafish genetic research inefficient and time consuming, and are termed as a genotyping bottleneck. Since mutant zebrafish provide the basis for a wide variety of drug screens. Fish with known mutations mimicking human diseases are valuable in that a drug that "cures" these fish could potentially be effective in humans. Mutants can also be developed that enable "tagging" of proteins and self-signaling of specific phenotypes or genotypes. Knowledge of specific mutants can also help with phenotyping and developments in functional genomics. It is critical for experimental biology to identify mutants with specific genes to understand biological processes. Further, being able to track the genotype of embryos is important for characterizing disease pathophysiology.

Zebrafish embryos that are 1 to 2 days old range from 600 μm (without chorion) and 1.2 mm (with chorion) [5]. A chorion is a protective bag that contains fluid (called the chorionic fluid) that surrounds the embryo at its birth and naturally lasts until it is 2 days old. Despite owing to their considerable large size (with reference to microscale)

microfluidic research tools involving zebrafish embryos have been made for (1) continuous monitoring of zebrafish embryo development under different drug gradients [1], [6], (2) observing normal development of zebrafish embryos [2], (3) droplet-based manipulation of live zebrafish embryos in digital microfluidics [7], (4) patterned delivery and expression of gene constructs in zebrafish embryos through electroporation to form desired mutants [8]. However, no work has been done to address the genotyping bottleneck for zebrafish research where microfluidic technology can play a significant role. With the ability to precisely control the movement of small volumes of fluid and living organisms contained in the fluid, microfluidics can help collect genetic material from zebrafish embryos while they reside in an environment (small fluid volumes) very similar to their natural environment. This capability increases the survivability of the fish and also provides more process control to the researcher.

This work introduces two types of microfluidic devices that are made in PDMS using laser ablation of adhesive films. Both of these devices help to resolve the genotyping bottleneck in zebrafish genetics-based research associated with the time-consuming process of DNA collection from zebrafish embryos that are 1 to 2 day old while also preserving the life/health of the embryo. One device collects the chorionic fluid as the genetic material is referred as “chorionic-fluid chip.” The other device collects fin tissue as the genetic material and is referred as “fin-clip chip.” The underlying functional methods by which these two devices work are referred as “chorionic-fluid method” and “fin-clip method,” respectively.

Methods and Materials

Chorionic-fluid Method and Chip Design

There are three steps for this procedure. First, zebrafish embryos at 24 hpf (hours postfertilization) are exposed to pronase solution for 5 to 6 minutes at room temperature (22 ºC). Pronase is a proteolytic enzyme that softens the chorion surrounding the embryo [9]. Pronase solution is prepared by mixing 30mg/ml of commercial Pronase (Part #. P-5147, Sigma-Aldrich, MO) in 1 ml of E3 buffer. E3 buffer is used by zebrafish researchers to breed the fish.

Secondly, the embryos are washed with E3 as pronase overexposure is harmful for embryos. This is done by exchanging the pronase solution containing the embryos with fresh E3 buffer three times.

In the final step the embryos are collected individually by suction in tubing ([~5 cm long] Part #06422-02, Cole Parmer Instrument Company, IL) connected to a disposable 3-ml syringe; only one embryo is collected in each tubing. Caution is taken that during suction the embryo (along with the E3 buffer around it) does not enter or touch the syringe-tip. Then the free end of the tubing is connected to the inlet of a microchannel in the chorionic-fluid chip. The microchannel is designed so that its width tapers from 2 mm at the inlet to 0.75 mm at the outlet, the height remaining constant at 1.7 mm (further details in Fig. 4.1). A typical size of a zebrafish embryo is approximately 600 µm/0.6 mm (without chorion) or 1200 µm/1.2 mm (with chorion) [5]. Hence, the channel design allows shear forces to act on the chorion, but not on the embryo when it separates from the chorion, thereby keeping the embryos safe from harm.

Once the tubing is connected to the microchannel inlet, pulsating pressure is applied

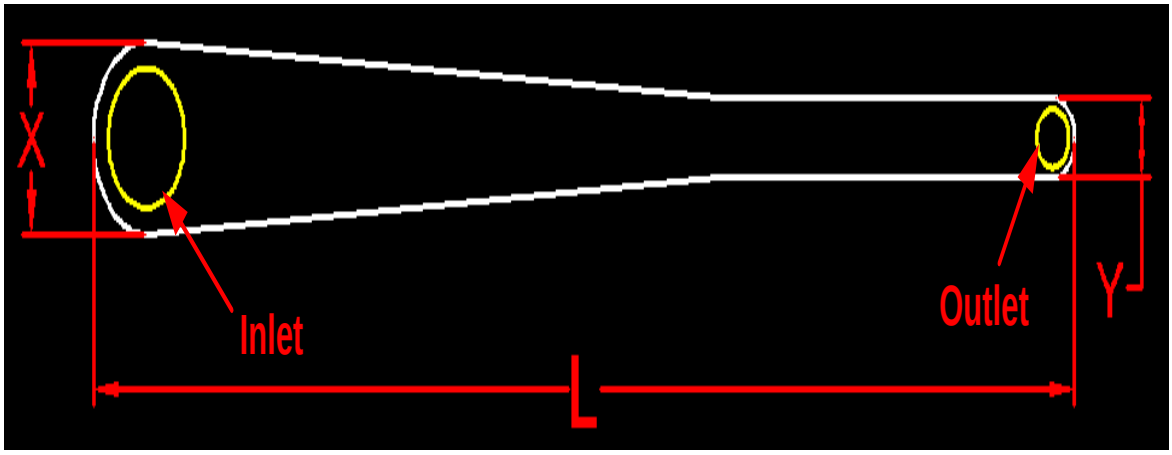

Figure 4.1. Microchannel design for chorionic-fluid method. This is the top view of the channel. Channel outline is in white, with inlet/outlet ports depicted in yellow and labels in red. The embryo enters from left to right. Approximate channel dimensions for L, X, W are 20 mm, 2 mm, 0.75 mm, respectively, with a channel height of 1.7 mm.

on the syringe's plunger by gently tapping the end of the syringe's plunger with a finger. This generates a pulsating flow inside the microchannel making the embryo travel across the microchannel in a series of small movements. The pulsating flow provides time to the embryo to adjust its body with varying microchannel width and avoid any harm to the embryo. Eventually the chorion tears and releases the chorionic fluid. When the embryo surfaces out of the microchannel at the outlet along with a small amount of fluid, the fluid (~60 µl) around the live embryo is collected manually using a pipette. The live embryo is separately collected by another pipette.

The tubing is then discarded and new tubing is used for the next embryo, which undergoes the same process described earlier, but in a new/unused microchannel (each chorionic-fluid chip contains 10 identical microchannels to process 10 different embryos). This reduces the chance of DNA contamination between different embryos.

The collected fluids (a mixture of chorionic fluid and E3) from processed embryos are then analyzed by standard genotyping techniques (polyermerase chain reaction [PCR] and high resolution melting analysis [HRMA]) and associated commercial hardware to genotype embryos of interest.

Fin-clip Method and Chip Design

Fig. 4.2(a) shows the design of the microfluidic chip used for fin-clip method. The chip is made in PDMS by replica molding from micromolds made from laser cutting of adhesive vinyl films.

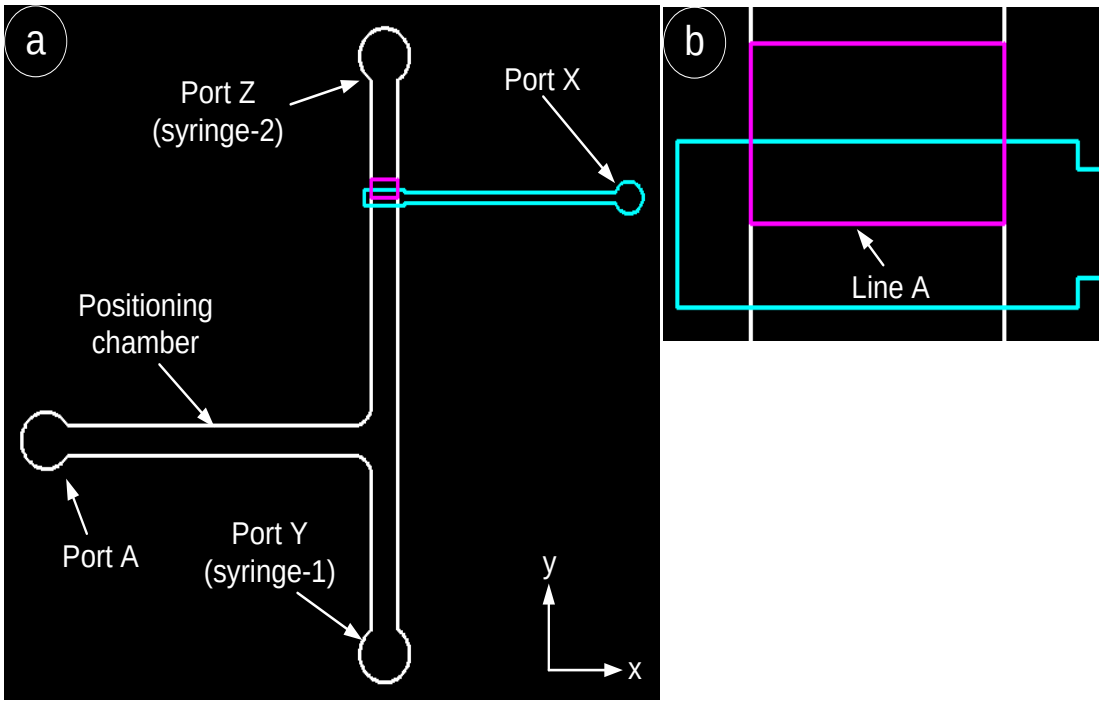

Figure 4.2. A 2D drawing for the fin-clip chip design. (a) The complete fin-clip chip design. (b) Expanded view of a part in the flow channel, including clipping chamber and depicting Line A.

The chip has two parts: a flow channel (highlighted in white and magenta) and a pneumatic channel (highlighted in cyan). The flow channel is ~700 μm wide and has two levels of heights: ~550 μm (highlighted in white in Fig. 4.2a) and ~220 μm (highlighted in magenta in Fig. 4.2a which is the clipping chamber, where the fin is clipped). The pneumatic channel is ~110 μm high with two parts of different widths (~350 μm and ~200 μm). The wider part (~350 μm) interfaces with the flow channel and is used to pneumatically actuate a membrane in the clipping chamber. The 350-μm width is selected based the stiffness of membrane (quantified in Chapter 3) to provide a balance of membrane deflection and membrane strength to avoid membrane failure and perform fin clipping of embryos.

The chip is operated manually by two syringes and an external pneumatic line connected to pneumatic channel at port X in Fig. 4.2. The other two syringes are used to control the position of the embryo in the flow channel and are therefore connected at ports Y and Z in (Fig. 4.2a). Port A is always open to the environment to provide access to air, extra E3 buffer, collection of fin tissue, and fin-clipped embryo.

An embryo is collected in tubing (Part #06422-02, Cole Parmer Instrument Company, Vernon Hills, IL, USA) connected to syringe-1 by suction. Then the outlet of the tubing is connected to port Y. The outlet of syringe-2 is attached to identical tubing, and the other end of the tubing is connected at port Z. The external pneumatic line is connected at port X.

Now it is required that the embryo enters the clipping chamber with its tail facing the chamber. However, there are two possible positions in which an embryo can enter at port Y: head-first or tail-first. If the embryo enters tail-first, then it is transferred

straight to the clipping chamber by simultaneous application of positive pressure from syringe-1 and negative pressure from syringe-2. If the embryo enters head-first, it is transferred to the positioning chamber first (shown in Fig. 4.2) by only the supply of positive pressure from syringe-1, and then by only application of negative pressure from syringe-2 the embryo is transferred to the clipping chamber. The dimensions of the flow channel are such that the embryo cannot flip in any direction at its own will, yet still move comfortably in the channel.

For a particular run, the fin-clip chip is placed under microscope so that the position of the embryo can be observed. The entire flow channel is initially filled with E3 buffer, and the embryo enters from port Y. Once the embryo reaches the clipping chamber with the appropriate position, the membrane is actuated as soon as point B on the embryo is at level with Line A in the clipping chamber. Point B is where the caudal blood artery connects with the caudal blood vein, which is about 300 μm from the tip of the tail at ~35 hpf (hours post-fertilization). When the membrane comes down on the embryo's tail its natural reaction is to escape in the negative y-direction (according to Fig. 4.2). This reaction results in clipping of a thin portion of its fin, which is just below the caudal blood artery. Then the embryo and the clipped tissue are both transported to port A sequentially (using actuation from the two syringes) where both are collected by a pipette for further analysis. However, while collecting the clipped tissue the pipette inevitably collects ~10 μl of E3 buffer. The chip is thoroughly cleaned with ethanol and deionized water after fin-clipping of 5 embryos.

PDMS Preparation

All PDMS used in this work had a base to crosslinking agent ratio of 10:1. After mixing the appropriate volume (based on number of chips to be made), the mixture is placed in a moderate vacuum chamber at 88 kPa to degas. Once degassed the PDMS is ready to be used.

Fabrication of Chorionic-fluid Chip

The chorionic-fluid chip is made by replica molding of PDMS in two parts. The first part contains the microchannel that is used to dechorionate the embryo (the mold for this part is referred as mold-I). The second part is basically a slab of PDMS (the mold for this part is referred as mold-II). Both of these parts are bonded together in the end to fully realize the chorionic-fluid chip. The mold-I is made by laser ablation of adhesive vinyl film (Gerber Instachange Removable Film, Gerber Scientific Products, Tolland, CT, USA) as described in Chapter 3. Once the pattern is cut it is adhered on the internal surface of the petri dish (Part #. 25384-302, VWR, PA).

Next, an appropriately sized 1.5-mm thick sheet of PMMA (Acrylite FF (clear), 0.06 inch thick, Evonik Industries, Essen, Germany) is bonded to a layer of double-sided tape (Product #. S-17844, 3M, MN) that is ~ 0.1 mm thick (without the carrier). The carrier of the double-sided tape is not removed. Afterwards the same pattern (that was cut in the adhesive vinyl film) is cut through the sheet of PMMA (with an adhered layer of double-sided tape) by laser ablation. The setup for this process is shown in Fig. 4.3. The laser ablation settings are tuned so that a small amount of tape carrier remains unablated. This keeps the cut pattern from falling off into the base of the laser bed.

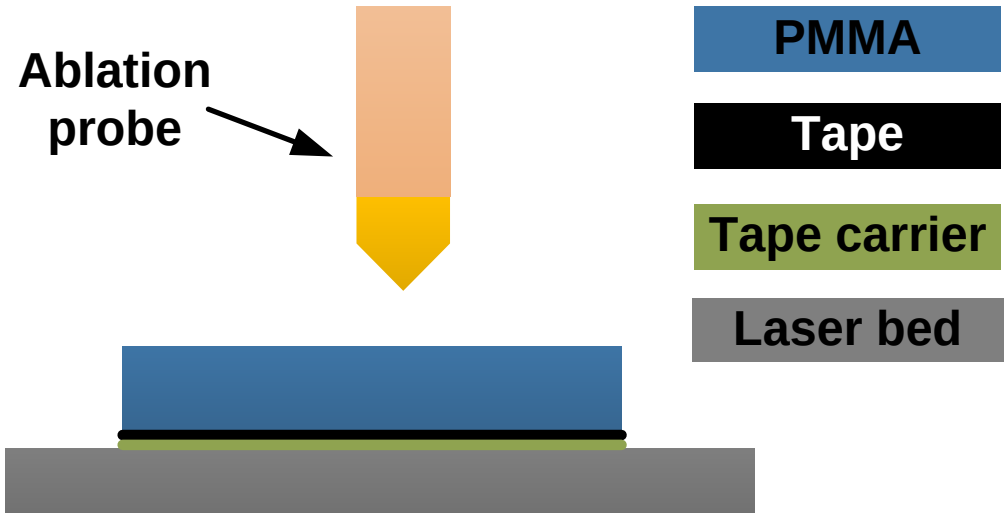

Figure 4.3. Setup of laser ablation for patterning PMMA/double-sided tape

Alternatively, a flat thin sheet of any material (that is not transparent to the wavelength of the laser) could be placed in between the PMMA sheet and the laser bed. After removing the tape's carrier, the cut PMMA pattern is adhered on the film pattern by the help of tweezers for the realization of the micromold.

Fig. 4.4 shows this arrangement of different layers of material to make the micromold. It is possible to directly stick the PMMA pattern to the petri dish surface to make the final mold. However, by having a mold with a previously placed patterned adhesive film can help in creating multirelief molds by attaching PMMA laser-ablated patterns (or solid object printed patterns) where required. A complete fabrication sequence of the chorionic-fluid chip is shown in Fig. 4.5. After the mold has been fabricated PDMS is poured over mold-I and into an identical empty petri dish (mold-II) to a thickness of ~6 mm from the base of the petri dish.

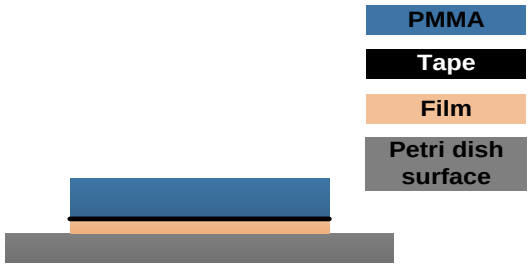

Figure 4.4. Different layers of material for micromold for chorionic-fluid chip.

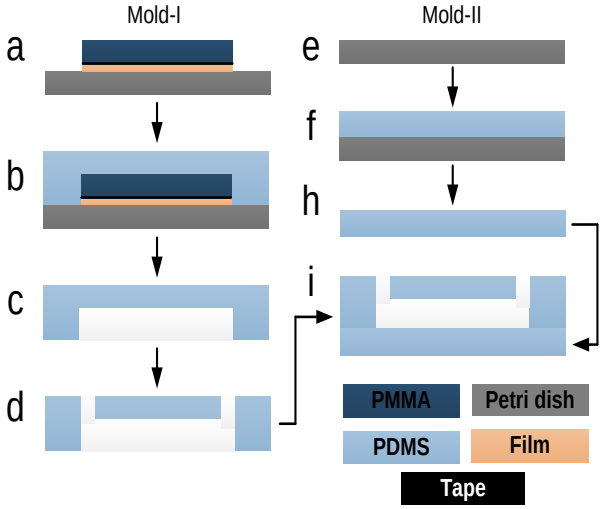

Figure 4.5. Fabrication schematic for the chorionic-fluid chip

After ensuring that the poured PDMS is free of air bubbles, these molds are placed in the oven at 62 ºC for at least 5 hours. This cures the PDMS into a solid. Later the molded PDMS pieces are removed and holes (3.5 mm diameter) are cored into microchannel using a biopsy punch (Part #. 15079, Ted Pella Inc., CA) for inlet and outlet. In the end the pieces are bonded together (in the arrangement shown in Fig. 4.5i) by corona bonding.

3D CO_2 Laser Ablation of Adhesive Vinyl Films for Micromolding

The CO_2 laser ablation of adhesive vinyl films presented in Chapter 2 is now extended for the fabrication of multirelief micromolds, previously introduced by Luo et al. [10]. The principle behind this fabrication process is selective laser ablation. Selective laser ablation is a type of subtractive micromachining process in which the laser properties are varied to achieve different depths of cut in the work piece so as to selectively remove material. Selective laser ablation has already been used in processing semiconductor devices [11]–[13]. In this case, the work piece is a single laminated layer of multiple adhesive vinyl films (Gerber Instachange Removable Film, Gerber Scientific Products, Tolland, CT, USA). Fig. 4.6 depicts the selective laser ablation process of a laminate of four adhesive vinyl films. The laminate is made by peeling of carriers from three films and placing them on top of the fourth film (with its carrier not removed). Then the laminate is placed on the laser ablation bed (Fig. 4.6a).

The CO_2 laser (VLS 3.60, Universal Laser Systems, AZ) used in this work has three parameters that can be adjusted depending on the material to be ablated. These are power, probe speed, and intensity. Once the laser is focused, tests are carried out by varying one or two of the three laser parameters to achieve the desired depth of cut.

In this case for a four-film laminate of adhesive vinyl film, the laser parameter values are

- Ablation to a depth of two films: power = 6%, probe speed = 10%, and intensity = 1000 pulses/inch
- Ablation to a depth of four films: power = 8%, probe speed = 10%, and intensity = 1000 pulses/inch

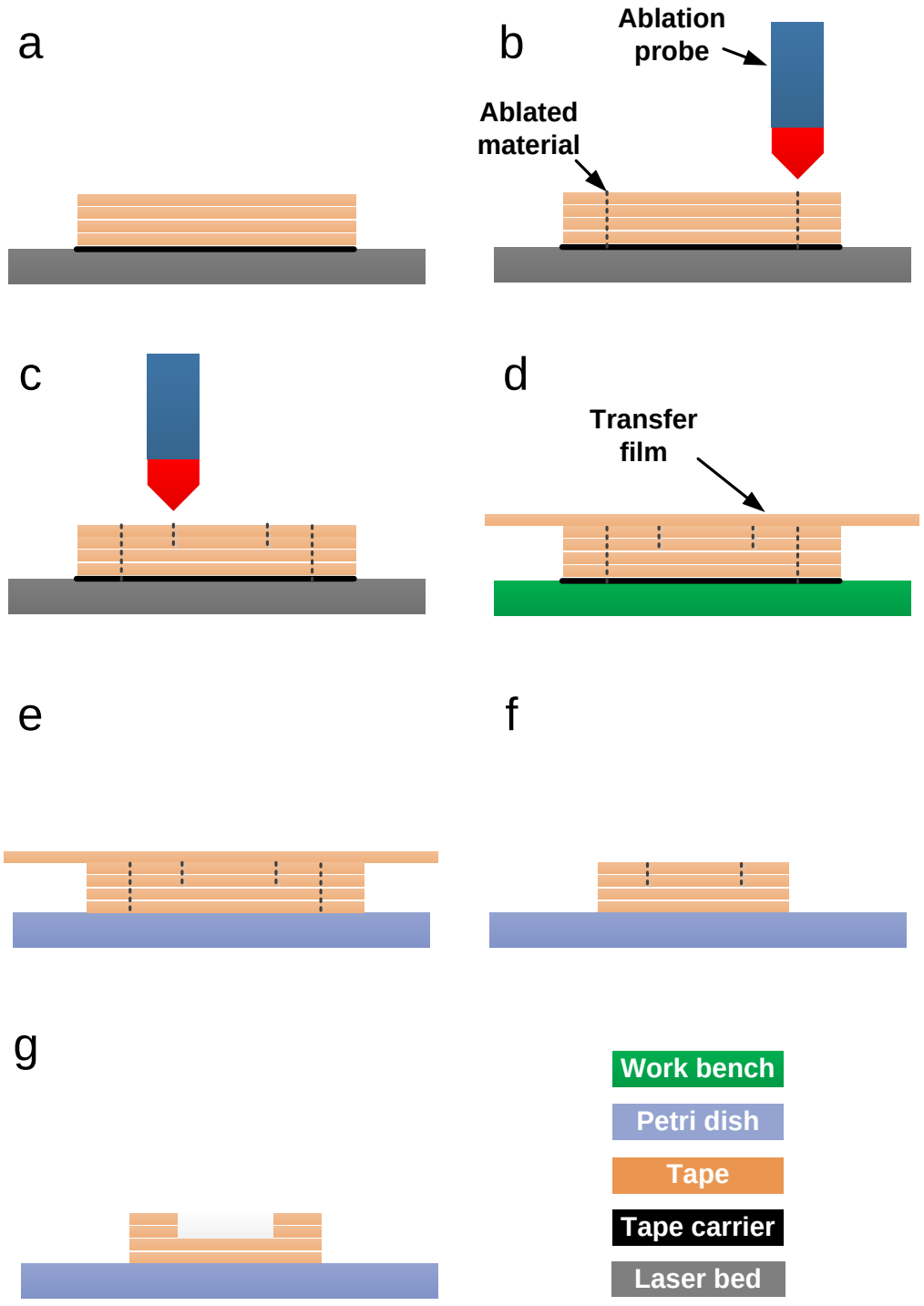

Figure 4.6. Fabrication schematic of 3D CO2 laser ablation of adhesive vinyl films

In laser ablation systems a 2D ablation pattern is initially drawn in a CAD (computer aided design) program. In this work AutoCAD (Autodesk Inc., CA, USA) was used to design 2D drawing of the pattern. The laser system includes a firmware that provides the flexibility to change the three parameters of a particular laser ablation process by line color of the drawing. Hence, the user can control the depth of cut during the entire laser ablation process of one drawing.

Once the laser is focused and laser parameters are set according to the line color of the drawing, the ablation process is executed (Fig. 4.6b and Fig. 4.6c). The ablated laminate is taken from the laser bed and placed on top of working bench. Then a single film (with the carrier removed) is stuck on top of the ablated laminate (Fig. 4.6d). This film is called the transfer film, and it helps in inhibiting "free regions" (where the laminate has been ablated all the way through) from dislocating when the laminate is transferred and stuck inside a petri dish by peeling off the bottom carrier (Fig. 4.6e). Then the transfer film along with unwanted laminate material is removed by tweezers (Fig. 4.6f). The laminate is rolled by a small roller to improve adhesion to the petri dish. Next, by the help of tweezers, the regions that were ablated to a depth of two films are removed (Fig. 4.6g). Similarly, an ablated pattern cut all the way through in an adhesive film laminate can be transferred by tweezers on another adhesive film or laminate to make multirelief micromolds.

Fabrication of Fin-clip Chip

The fin-clip chip is made by replica molding of PDMS. The micromold for the fin-clip chip is made by 3D CO_2 laser ablation of five-film adhesive vinyl films (Gerber

Instachange Removable Film, Gerber Scientific Products, Tolland, CT, USA) as described earlier. As shown in Fig. 4.2, the fin-clip chip has two parts: a flow channel (highlighted in white and magenta) and a pneumatic channel (highlighted in cyan). Fig. 4.7 shows the fabrication schematic of flow channel from part(a) to part(f), pneumatic channel from part(g) to part(i), and the final chip in part(k).

The mold for the flow channel (Fig. 4.7a) is made by fabrication techniques

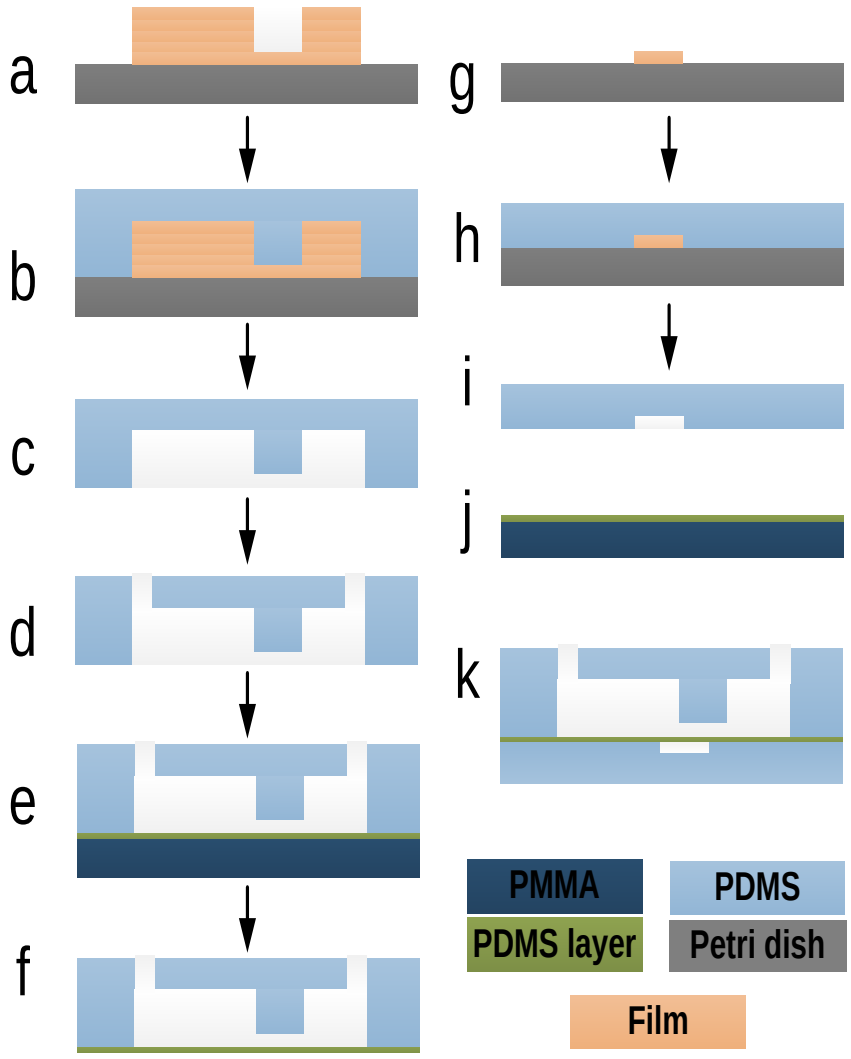

Figure 4.7. Fabrication schematic for fin-clip chip

described in the previous section by using a laminate of five films (each film ~110 μm thick). Once the mold is made, uncured PDMS is poured in the mold (Fig. 4.7b). After ensuring that the poured PDMS is free of air bubbles, the mold is placed in the oven at 62 ºC for at least 5 hours. Then the cured PDMS is removed from the mold (Fig. 4.7c). Holes (~1.5 mm diameter) for ports A, X, Y, Z (according to Fig. 4.2) are cored in the molded PDMS piece (Fig. 4.7d) to complete the fabrication of flow channel layer. The coring tool is biopsy punch (Part #. BP15, HealthLink, FL).

To make the actuating membrane, 5 ml of uncured PDMS is spun on a PMMA 4-inch wafer at 2800 rpm for 60 seconds at a ramp of 340 rpm/s and then baked in an oven at 62 ˚C for at least 1.5 hours (Fig. 4.7j). This generates a PDMS layer of 16.4 ± 0.9 μm thickness.

The PDMS layer (overlying the PMMA wafer) is bonded (by corona discharge [14]) to the flow channel layer and placed in the oven at 62 ˚C for 30 minutes as shown in Fig. 4.7e. Afterwards the flow channel layer along with the bonded actuated membrane is separated from the PMMA wafer (Fig. 4.7f).

The mold for the pneumatic flow layer is fabricated by laser ablation of a single adhesive vinyl film as described in detail in Chapter 3 and depicted in Fig. 4.7g (mold), Fig. 4.7h (uncured PDMS poured in the mold and cured), and Fig. 4.7i (cured PDMS pneumatic flow layer separated from the mold).

In the end, the flow channel layer and the pneumatic flow layer are bonded by corona discharge in the arrangement shown in Fig. 4.7k to fully realize the fin-clip chip.

Tests for Chorionic-fluid Method and Fin-clip Method

Based on the described methods, experiments were performed to determine the following important aspects of the work:

1. The ability of both methods to collect the genetic material without damaging the embryo;
2. The presence of enough DNA in chorionic fluid for genotyping embryos;
3. The source of the DNA from the chorionic fluid (maternal or embryonic).

For testing the chorionic-fluid method, a cross of wild-type male fish to females heterozygous was used for a Gal4-transgene. The Gal4-transgene is on a Tol2-transposon carrying a transgenesis marker of GFP (Green Fluorescent Protein) expressed in the heart. So embryos are either wild-type (GFP-negative) or Gal4+ (GFP-positive). After collecting chorionic fluid samples from these two groups of fish, PCR and HRMA were carried out on the samples.

For testing the fin-clip method, fin tissue from 6 Gal4+ embryos was collected using the method described earlier. After collection, conventional DNA extraction, PCR, and HRMA are carried out on the samples.

For viability tests, wild-type embryos were processed through both methods. The embryos were observed for 5 days. Additionally, 3 wild-type fish had their fins clipped by the fin-clip method and were monitored at room temperature of 22 ˚C for 5 days for fin regrowth. Furthermore, sensitivity tests were performed for both methods consisting of a sample pool of 18 embryos for chorionic fluid method and 15 embryos for the fin-clip method.

DNA Extraction for Fin-clip Method

The collected volume of 10 µl of E3 buffer (containing the clipped tissue) is placed in a 40 µl volume of DNA lysis buffer in a tube. About 5 µl of Proteinase K (10 mg/mL) (Part # 03115879001, Roche Applied Science, IN, USA) is inserted into the tube, and the tube is placed in a water bath at 50 ˚C for 4 hours to digest all proteins and cellular components. In the end the tube is placed in a boiling water bath for 15 minutes to denature Proteinase K enzyme.

PCR and HRMA

Before PCR or HRMA, the samples in tubes (only for the chorionic fluid method) are placed in a boiling water bath for 10 minutes to denature any Pronase enzyme. PCR reactions were performed in 96-well, hard-shell plates (Part#. HSP9665, Bio-Rad Inc., CA, USA) in 10 µl volume: 2 µl of master mix (Lightscanner 5x Master Mix, Biofire Diagnostics Inc., UT, USA), 1 µl of 5 µM forward primer, 1 µl of 5 µM reverse primer, and 6 µl of sample DNA. HRMA was carried out on a 96-well LightScanner instrument from Biofire Diagnostics, Inc. Table 4.1 lists the parameters used for PCR and HRMA and the set primers.

Table 4.1

PCR and HRMA parameters for two sets of primers used in chorionic fluid method and fin-clip method

Forward Primer	**Reverse Primer**	**Amplicon**	**Cycling parameters**	**N (cycles)**	**HRMA temperature range**
AAAAACC GAAGTGC GCCAAG	GGAGAGT AGCGACA CTCCCAG	AAAAACCGAA GTGCGCCAAG TGTCTGAAGA TGTTGACCCT CACAGCGATG AGAGG	95ºC for 30 seconds, followed by 'N' cycles of 94ºC at 5 seconds, 68ºC at 5 seconds, 72ºC at 5 seconds and in the end cooled to 5ºC	35 (60 cycles for chorionic fluid method only)	72ºC to 94ºC

Results and Discussion

Micromolds and Fabricated Chips

Fig. 4.8 shows micromolds and fully fabricated zebrafish genotyping chips. Only two films have been simultaneous ablated by the 3D laser ablation process to make a micromold for the flow channel of the fin-clip chip Fig. 4.8(e).

Laser ablation can create significant debris and therefore, the ablation process can get inconsistent beyond simultaneous ablation of two or three films. However, this limitation could be overcome by generating patterns from laminates of two or three films and then stacking them on top each other or other patterned films that are already adhered to the petri dish. It is pointed out that these micromolds can only be used for rapid prototyping of PDMS microfluidic devices that contain channels at different heights. Therefore, the process is designed to build micromolds for single use and may have low resolution for a significant number of applications of microfluidics.

The strength of these molds can be increased and therefore, their multipleuse can be possible by using films with stronger adhesives. Secondly, since laser ablation was used to pattern the films, the molds do not have smooth walls. Smooth walls could be essential in considerable number of microfluidic applications, and so micromolds made from the described laser ablation process would not be desirable.

Chip Design and Genotyping

Tests carried out with a chorionic-fluid chip to determine the source of chorionic DNA showed that wild-type embryos did not show PCR amplification, demonstrating that no maternal cells / DNA was contained in the chorionic fluid (Fig. 4.9).

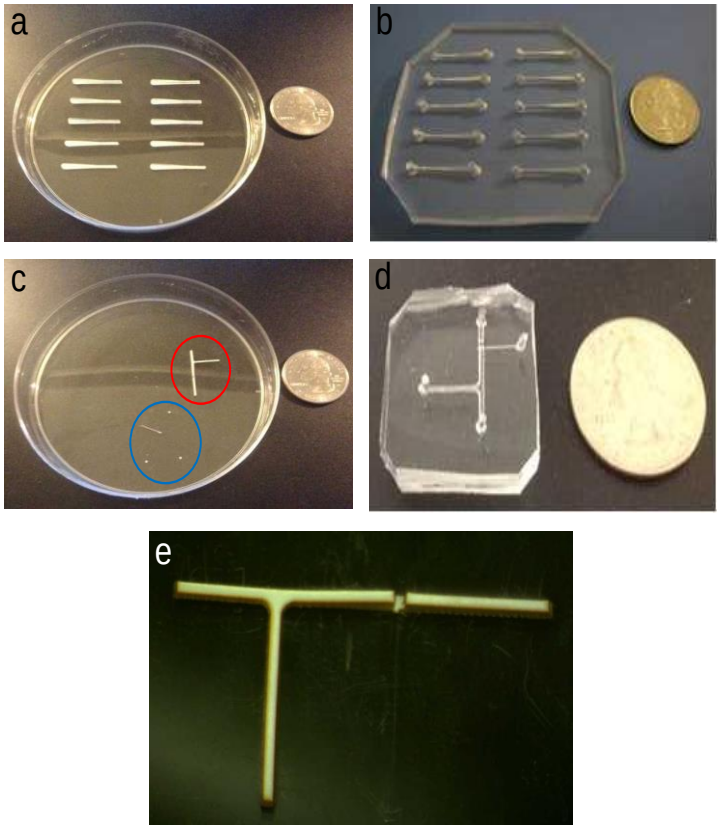

Figure 4.8. Micromolds and fully fabricated chips alongside a US quarter coin; (a) micromold for chorionic-fluid chip; (b) fully fabricated chorionic-fluid chip with 10 separate chambers for chorionic fluid extraction; (c) micromold for fin-clip chip. The mold for the flow channel is highlighted by a red circle and the mold for the pneumatic channel is highlighted by a blue circle; (d) fully fabricated fin-clip chip; (e) a magnified picture of the mold for the flow channel of the fin-clip chip

Conversely, all transgenic embryos' DNA was successfully amplified. When 18 embryos were processed through the chorionic-fluid method, the sensitivity was 78%. This is most likely due to the low quality of chorionic fluid as a genetic material for genotyping. Furthermore, it could be observed based on the large number of PCR cycles required (60 cycles) for appropriate amplification of chorionic DNA (as shown in Table 4.1).

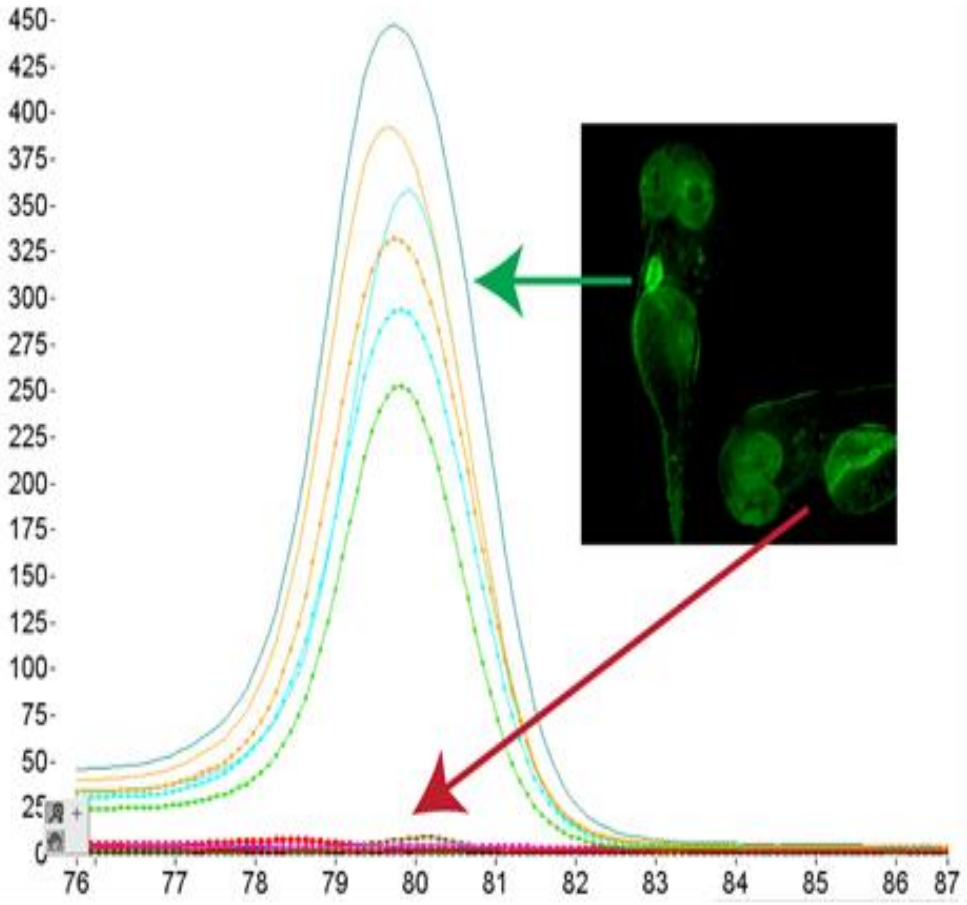

Figure 4.9. HRMA plots of DNA collected from chorionic-fluid method

The low quality of chorionic fluid as a genetic material for genotyping places further stringent demands on the collection of chorionic DNA, which in turn is reflected on the design of the chorionic-fluid chip. Therefore, the collected chorionic-fluid should have minimum dilution by E3 buffer that is used to push the embryo across the channel by pulsating flow. However, since this pulsating flow is generated manually, it can negatively affect the sensitivity of the device by excessive dilution of DNA.

On the other hand clipped fins have been a conventional source of DNA to genotype zebrafish [3]. Fig. 4.10 shows the results of genotyping a set of 6 different embryos using the fin-clip chip. The sensitivity of this protocol determined from processing 15 different embryos was 100%. Though the fin-clip method has better sensitivity the appropriate positioning of the embryo in the clipping chamber is crucial to clip the fin without damaging the embryo. Therefore, this process requires continuous awareness of the position of the embryo inside the chip and associated use of syringe pumps.

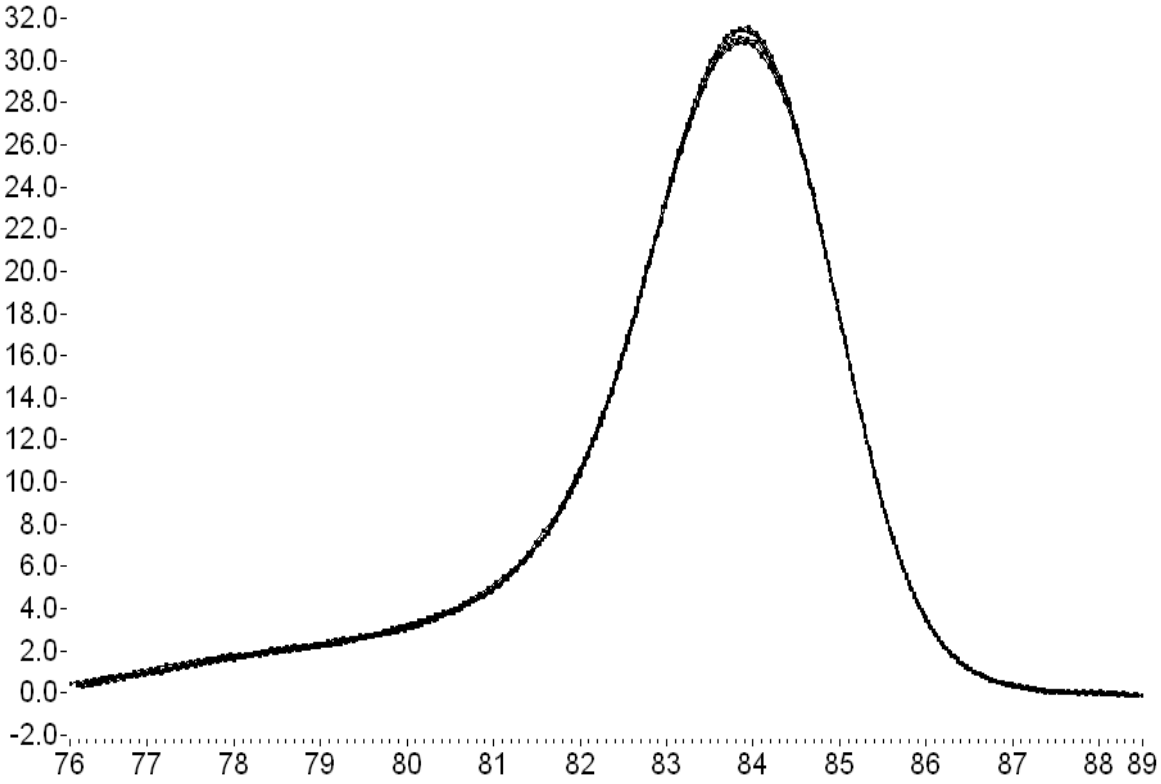

Figure 4.10. HRMA plots of DNA collected from fin-clip method

Since the embryo is not anesthetized, it will try to move away from the chamber as it is drawn into it. However, further research into the design of the protocol can help create fluid or structural obstacles that can help restrict embryo's movements. This will help in automating this process. Nonetheless, this work reveals a proof-of-concept technique to help preserve the life of zebrafish embryo in early stage genotyping. Viability results show 100% viability for both methods (Table 4.2) as the embryos showed sensitivity to touch with normal swimming behaviors and had normal morphological development.

Additionally, 3 wild-type fish had their fins clipped by the fin-clip method and were monitored for fin regrowth at room temperature of 22 ºC for 5 days (Fig. 4.11).

Table 4.2

Viability statistics for both methods

Method	**Embryos (#)**	**Embryos with 100% viability (#)**
Chorionic fluid method	20	20
Fin-clip method	16	16

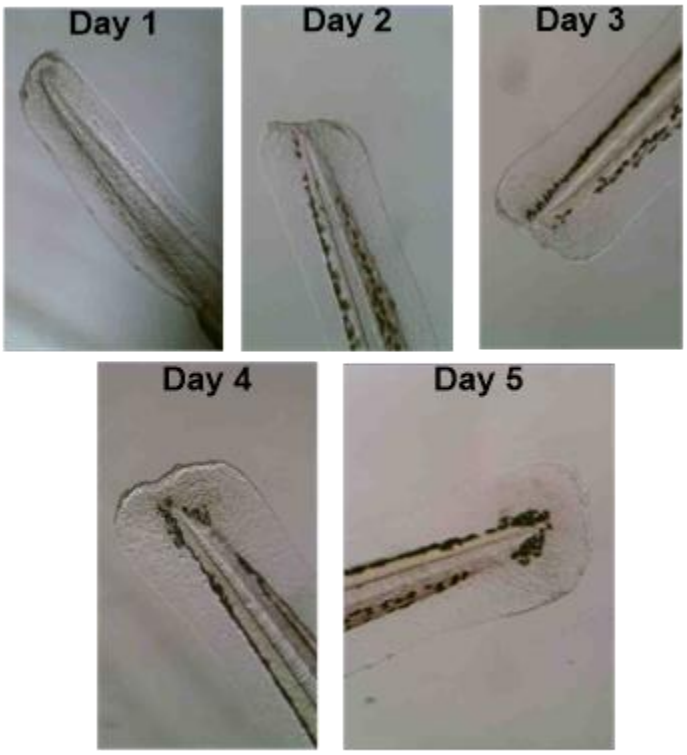

Figure 4.11. Fin regrowth of a wild-type zebrafish embryo in a period of 5 days

Conclusion

In this presentation laser ablation of adhesive vinyl films was used to fabricate micromolds. Observations show that simultaneous laser ablation of 2 or 3 films will provide consistent ablation results, beyond which debris from ablation becomes considerable to interfere with ablation process.

Two types of microfluidic chips for collection of genetic material from zebrafish embryos (1 to 2 days old) have been developed: chorionic-fluid method and fin-clip method. Results show that both methods provide an ability to preserve embryo's life while determining its genotype at an early stage and can therefore increase the use of

zebrafish embryos in biomedical research. The results also reveal that the source of chorionic DNA is embryonic and that chorionic-fluid method would require further optimization for higher sensitivity. Further research can help scale these methods for high-throughput genetic screening, which could complement the cost-effectiveness of using zebrafish disease models.

References

[1] Choudhury, D., van Noort, D., Iliescu, C., Zheng, B., Poon, K., Korzh, S., Korzh, V., and Yu, H., 2012, "Fish and Chips: a Microfluidic Perfusion Platform for Monitoring Zebrafish Development," Lab Chip, **12(**5), pp. 892–900, doi: 10.1039/c11c20351g

[2] Wielhouwer, E. M., Ali, S., Al-Afandi, A., Blom, M. T., Olde Riekerink, M. B., Poelma, C., Westerweel, J., Oonk, J., Vrouwe, E. X., Buesink, W., Vanmil, H. G. J., Chicken, J., Oever, R. V., and Richardson, M. K., 2011 "Zebrafish Embryo Development in a Microfluidic Flow-through System," Lab Chip, **11**, doi: 10.1039/c01c00443j

[3] Westerfield M., 1995, *The Zebrafish Book*, University of Oregon Press, Eugene, OR

[4] Parant, J. M., George, S. A., Pryor, R., Wittwer, C. T., and Yost, H. J., 2009, "A Rapid and Efficient Method of Genotyping Zebrafish Mutants," Dev. Dyn., **238**(12), pp. 3168–3174, doi: 10.1002/dvdy.22143

[5] Wang, W., Liu, X., Gelinas, D., Ciruna, B., and Sun, Y., 2007, "A Fully Automated Robotic System for Microinjection of Zebrafish Embryos," PLoS One, **2**(9), p. e862, doi: 10.1371/journal.pone.0000862

[6] Yang, F., Chen, Z., Pan, J., Li, X., Feng, J., and Yang, H., 2011, "An Integrated Microfluidic Array System for Evaluating Toxicity and Teratogenicity of Drugs on Embryonic Zebrafish Developmental Dynamics," Biomicrofluidics, **5**(2), pp. 24115, doi: 10.1063/1.3605509

[7] Son, S. U., and Garrell, R. L., 2009, "Transport of Live Yeast and Zebrafish Embryo on a Droplet Digital Microfluidic Platform," Lab Chip, **9**(16), pp. 2398–2401, doi: 10.1039/b906257b

[8] Bansal, T., Lenhart, J., Kim, T., Duan, C., and Maharbiz, M. M., 2009, "Patterned Delivery and Expression of Gene Constructs into Zebrafish Embryos using Microfabricated Interfaces," Biomed. Microdevices, **11**, pp. 633–641, doi: 10.1007/s10544-008-9273-5

[9] Kim, D. H., Sun, Y., Yun, S., Kim, B., Hwang, C. N., Lee, S. H., and Nelson, B. J., 2004, "Mechanical Property Characterization of the Zebrafish Embryo Chorion," 26th Ann. Int. Conf. IEEE EMBS, San Francisco, USA, **7**, pp. 5061–5064.

[10] Luo, L. W., Teo, C. Y., Ong, W. L., Tang, K. C., Cheow, L. F., and Yobas, L., 2007, "Rapid Prototyping of Microfluidic Systems using a Laser-patterned Tape," J. Micromech. Microeng., **17**(12), pp. N107–N111, doi: 10.1088/0960-1317/17/12/N02

[11] Knorz, A., Peters, M., Grohe, A., Harmel, C., and Preu, R., 2009, "Selective Laser Ablation of SiNx Layers on Textured Surfaces for Low Temperature Front Side Metallizations," Prog. Photovolatics, **17**, pp. 127–136, doi: 10.1002/pip.856

[12] Dhar, S., Barman, A. R., Ni, G. X., Wang, X., Xu, X. F., Zheng, Y., Tripathy, S., Rusydi, A., Loh, K. P., Rubhausen, M., Neto, A. H. C., Özyilmaz, B., and Venkatesan, T., 2011, "A New Route to Graphene Layers by Selective Laser Ablation," AIP Adv., **1**(2), pp. 022109, doi: 10.1063/1.3584204

[13] Haase, F., Garralaga, E., Bothe, K., and Brendel, R., 2011, "Layer Selective Laser Ablation for Local Contacts to Thin Emitters," Energy Procedia, **8**, pp. 577–580, doi: 10.1016/j.egypro.2011.06.185

[14] Samuel, R., Sant, H. J., Jiao, F., Johnson, C. R., and Gale, B. K., 2011, "Microfluidic Laminate-based Phantom for Diffusion Tensor-magnetic Resonance Imaging," J. Micromech. Microeng., **21**(9), pp. 095027, doi: 10.1088/0960-1317/21/9/095027

CHAPTER 5

CONCLUSIONS, CONTRIBUTIONS, AND FUTURE WORK

The dissertation reports on three applications of PDMS-based microfluidics in the field of neuroscience. This chapter lists conclusions, contributions, and opportunities of further work in each of these applications.

Fabrication of a Microfluidic Laminate MRI Phantom

Conclusions

- Results reveal the ability of highly patterned 10-μm thick PDMS layers (30 layers) to be manually staked on top of each other.
- Despite being a manual process, the layer stacking protocol is efficient enough to inhibit any chance of entrapped air bubbles between stacked layers. Furthermore, the fabrication protocol inhibits wrinkling of stacked layers despite the layers being very flexible and prestressed.
- Results show that despite the high hydrophobicity of PDMS, these microchannels can be filled by water when placed in an environment under a mild vacuum.

Contributions

- Stacking of these patterned thin layers is used to produce the first MRI Phantom for brain white matter to help in the development of more sensitive MRI machines.
- The PDMS multilayered fabrication technology developed in this application can be extended to build complex and more functional microfluidic devices.

Future Work

However, the fabrication process can be improved when carried out in a cleanroom environment and by utilizing aligners. The MRI Phantom stimulates brain white matter and hence, it is important to have well-defined anisotropy of diffusion of water molecules in the microchannels of the phantom. Since the phantom is a multilayered device, dust particles can get entrapped in between layers and change the microarchitecture and consequently disrupt anisotropic diffusion of water molecules. Carrying out the fabrication in a cleanroom environment can help in avoiding such interference from dust particles. Furthermore, the microarchitecture of the phantom can be more reproducible by the use of specialized aligners to align thin PDMS layers with respect to each other.

The MRI signals from the phantom were not uniform across the device and contained considerable noise. This could be attributed to the inability of current MRI technology to read from microchannels of such size, material characteristics of PDMS, and the unwanted involvement of dust particles in the microarchitecture of the device. Further work in these aspects could help improve the MRI signal-to-noise ratio.

Innovative Fabrication of PDMS-based Microvalve Arrays

Conclusions

- It was discovered that just by manipulating the stiffness of spin-cast PDMS membranes (incorporated in doormat-style microvalves) through the shape of the associated valve chambers, hundreds of doormat-style microvalves can be fabricated.
- Simulations revealed how the stiffness of the membrane varies with shape and size of the valve chamber, and associated experiments showed how this stiffness has a direct effect on the contact ratio between the membrane and the valve chamber. Realization of contact ratio is essential to the fabrication of these microvalve arrays.

Contributions

- The capability of this new fabrication protocol was demonstrated by building a microfluidic 32-well plate interface for high-throughput manipulation of *C. elegans.* Microvalves are common elements in PDMS-based microfluidic devices. The new fabrication technique to build 100s of doormat-style microvalve arrays outside a cleanroom facility would be useful for prototyping microfluidic devices.
- The simulation model can also be used in the design of other microfluidic devices where stiffness of spin-cast PDMS membranes is an important design parameter.

Future Work

It is anticipated that by decreasing the height of valve chambers (which was constant in this presentation) the contact ratio can be increased. This can help decrease

the valve chamber size for a particular contact ratio and facilitate more compact microvalve arrays. Hence, additional simulations and experiments to study the effect valve chamber height and shape on the contact ratio would be helpful.

Microfluidic Zebrafish Genotyping Chips

Conclusions

- In the fabrication of the multirelief micromold, results show that simultaneous ablation of two or three films is recommended for consistency, as ablation debris causes inconsistent ablation of four or more films.
- The zebrafish fin-clipping device was used to successfully fin-clip zebrafish embryos between the age of 24–48 hpf (hours post fertilization) and collect the clipped fin tissue for genotyping the embryo.
- It was shown that passing a zebrafish embryo (at 24 hpf with a presoftened chorion) through a constricted microchannel can rupture the chorion and release the chorionic fluid that can be collected at the outlet of the channel. This chorionic fluid can be used to genotype the embryo.

Contributions

- The zebrafish fin-clipping device was able to perform the fin-clipping procedure on the fish without damaging the embryos health, as the embryos were able to grow back their fins in 5 days and showed no signs of health defects. This capability of maintaining embryo’s health while collecting fin tissue from it is currently not possible with embryos less than 2 days old.

- The chorionic-fluid method can be used to genotype a zebrafish embryo, and results show that this protocol causes no harmful effect to the embryo's health.
- Results also show that the source of chorionic fluid for a particular embryo is embryonic and not maternal. However, this protocol is comparatively less efficient than the fin-clip protocol.
- This work reports that harm-free genotyping of zebrafish embryos is possible at an early age (24–48 hpf), which is currently not possible with any other model multicellular organism. This unique advantage in zebrafish can aid in solving key biomedical questions where zebrafish provide their unique set of traits as a model organism.

Future Work

Both zebrafish genotyping devices mentioned in this work are still manually operated. Additional research in manipulation of zebrafish embryos in these devices could help making the position of a live embryo more predictable/controllable to allow a degree of automation and therefore high throughput for fast genetic screens.